Characterization of ultrashort laser pulses: towards a cost-effective solution

João P. S. Rodrigues
Mestrado Integrado em Engenharia Física
Departamento de Física e Astronomia
2019

Orientador
Prof. Dr. Helder Crespo, Prof. Auxiliar, Dep. de Física e Astronomia, Fac. de Ciências

Coorientador
Dra. Rosa Romero, CEO, Sphere Ultrafast Photonics (Spin-off da U. Porto)

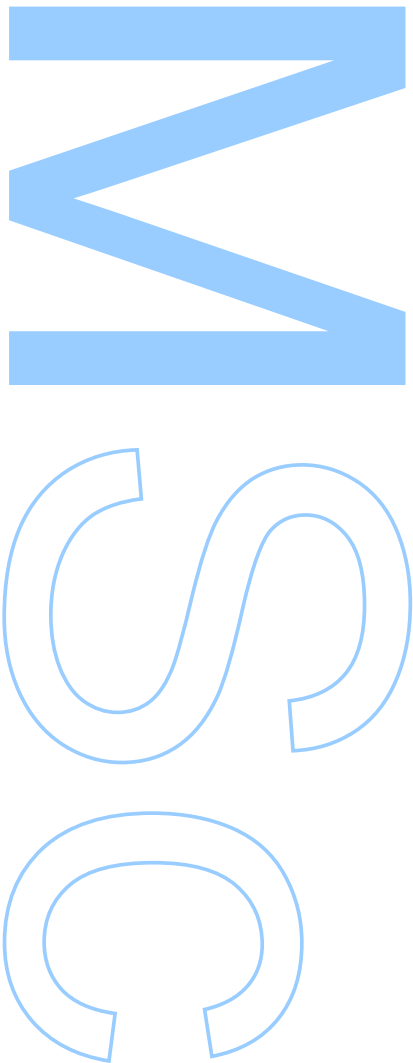

U.PORTO

FACULDADE DE CIÊNCIAS
UNIVERSIDADE DO PORTO

Todas as correções determinadas pelo júri, e só essas, foram efetuadas.

O Presidente do Júri,

Porto, _____/_____/_____

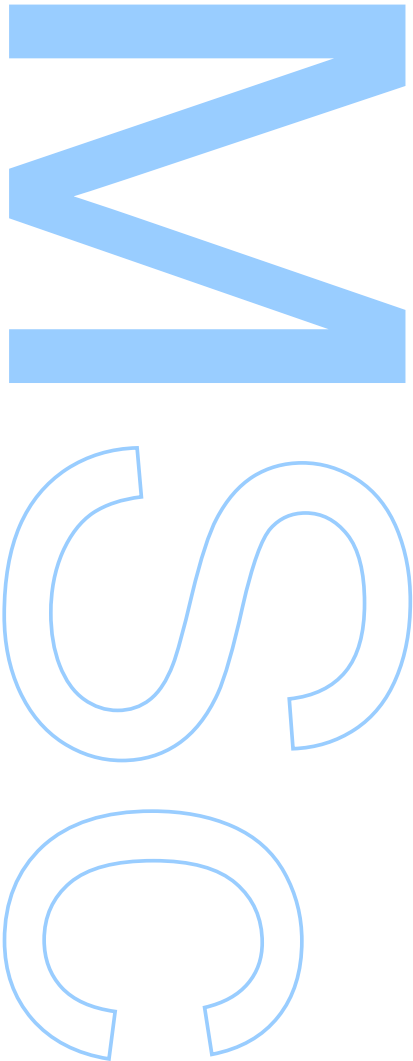

UNIVERSIDADE DO PORTO

MASTERS THESIS

Characterization of ultrashort laser pulses: towards a cost-effective solution

Author:
João P. S. RODRIGUES

Supervisor:
Prof. Dr. Helder CRESPO

Co-supervisor:
Dra. Rosa ROMERO

A thesis submitted in fulfilment of the requirements
for the degree of MSc. Engineering Physics

at the

Faculdade de Ciências da Universidade do Porto
Departamento de Física e Astronomia

February 6, 2020

"Persistence is very important. You should not give up unless you are forced to give up."

Elon Musk

Acknowledgements

The work reported in this thesis would have been an impossible task without the knowledge, guidance and support of many individuals. I would like to acknowledge some of them.

I am grateful to Prof. Helder Crespo for teaching me the theory behind lasers, which inspired me to follow this line of research.

I would also like to thank everyone at Sphere Ultrafast Photonics for making me feel at home in a professional work environment. I thank my co-supervisor, Dra. Rosa Romero, for always pressuring me to give it my all and obtain the best results possible. I would also like to acknowledge the help of Ricardo Moreira in software development and the contribute of Miguel Miranda in the testing of the developed devices.

A special thanks goes to Paulo Guerreiro for closely following the progress of this project, providing me with invaluable insight, guidance and feedback, without which the results here presented would certainly not have been attained.

Additionally, I would like to thank all my friends for all the special moments you have provided me with.

I give my sincere thanks to my family for supporting me, both emotionally and financially throughout the last five years. I hope I can someday pay it back.

A loving thanks goes to Catarina. For always being there when I needed you the most.

UNIVERSIDADE DO PORTO

Abstract

Faculdade de Ciências da Universidade do Porto
Departamento de Física e Astronomia

MSc. Engineering Physics

Characterization of ultrashort laser pulses: towards a cost-effective solution

by João P. S. RODRIGUES

Ultrashort pulses in the femtosecond (10^{-15}s) or even attosecond (10^{-18}s) regimes are of the utmost importance in many applications of modern science. However, even if one has a laser system capable of generating such short pulses, these bursts of energy are impossible to control and characterize using conventional techniques.

The d-scan products by Sphere Ultrafast Photonics are capable of fully retrieving the electric field of such pulses, enabling their compression down to the so-called Fourier limit. The technique has been used in many fields of research, including to achieve single-cycle pulses down to 2.2 fs. The work performed in this thesis aimed to develop custom devices which are essential for the d-scan technique.

Firstly, we designed PCBs capable of integrating a trigger signal in the d-scan products to synchronize the acquisition of the spectrometers with the pulses of low repetition rate lasers. These boards achieved opto-isolation of the input signal, conversion of this signal to adequate voltage levels (from TTL to LVTTL) and enable the control of an LED through the GPIO pins on the spectrometers. The PCBs have already been used to implement the trigger feature in multiple d-scan devices, proving the success of the development process.

We then developed a high precision translation stage to be used with the glass wedge pair required for the d-scan technique. This device was thoroughly tested using a Michelson interferometer to characterize the minimum step length (250 nm), which was shown to agree with the expectations with a 7.46 % error. The device also shows a standard deviation from the average step length of 23.5 %, when using the smallest possible step length, which is not expected to translate into larger step sizes such as the ones used during a d-scan measurement ($\sim$100 µm). This was later confirmed by performing several of

these measurements on a 7 fs Ti:Sapphire laser and observing that the retrieval algorithm provides consistent results for the RMS error (2 %), pulse width ($\sim$8.6 fs) and pulse peak power ($>$95 %). The production cost goal of 500 € was also achieved.

Finally, we developed a high resolution Indium-Gallium-Arsenide spectrometer, in the near-infrared wavelength range. This device was tuned to have a 3 nm resolution for the spectrum of a 1064 nm DPSS laser, demonstrating a signal strength of $\sim$80 % of saturation at an integration time of 100 µs. A wavelength calibration of the device was them performed resulting in an R^2 of 0.99998 and a spectral range of $[950.5 - 1722.5]$nm. The device was then calibrated in terms of intensity with the help of a white light lamp. By measuring the spectrum of a Mercury vapor lamp, we showed that the 3 nm resolution holds across the whole spectral range of the device. Spectra acquired by the developed spectrometer were also shown to be in agreement with the data obtained using a state of the art InGaAs spectrometer. The two devices are shown to have similar resolutions, with the developed one having a spectral range approximately 35 % larger than the commercial product. It is also worth noting that this is a highly compact device with a total size of 120 mm $\times$ 75 mm $\times$ 47 mm. Besides that, the production cost of the device was kept under the set budget of 3500 €.

UNIVERSIDADE DO PORTO

Resumo

Faculdade de Ciências da Universidade do Porto
Departamento de Física e Astronomia

Mestrado Integrado em Engenharia Física

Caracterização de impulsos laser ultracurtos: estudo de soluções de custo acessível

por João P. S. RODRIGUES

Impulsos ultracurtos no regime do femtossegundo (10^{-15}s) ou até mesmo do attosegundo (10^{-18}s) são da maior importância em diversas aplicações da ciência moderna. No entanto, mesmo que um sistema laser seja capaz de produzir estes impulsos, estas rajadas de energia são impossíveis de controlar e caraterizar através de técnicas de medida convencionais.

Os produtos d-scan da Sphere Ultrafast Photonics são capazes de recuperar na integridade o campo elétrico destes impulsos, permitindo a sua compressão até ao chamado limite de Fourier. Esta técnica tem sido usada em múltiplos campos de investigação, incluindo na geração de impulsos de um único ciclo óptico, com 2.2 fs de duração. O presente trabalho tem como objetivo o desenvolvimento de dispositivos especificados para uso com a técnica d-scan.

Primeiramente, foram desenhadas PCBs capazes de integrar um sinal de disparo nos produtos d-scan para a sincronização da aquisição dos espectrómetros com impulsos de lasers de baixa taxa de repetição. Estas placas permitem o isolamento óptico do sinal de entrada, a conversão do sinal para níveis the tensão adequados (de TTL para LVTTL) e o controlo de um LED através de um pino de GPIO dos espectrómetros. As PCBs já se encontram instaladas em alguns produtos d-scan, provando assim o sucesso do seu desenvolvimento.

De seguida, foi desenvolvida uma carruagem de translação de alta-precisão para ser usada com um par de cunhas de vidro na técnica d-scan. Este dispositivo foi caraterizado com um interferómetro de Michelson de modo a verificar o comprimento de passo mínimo (250 nm), o qual foi demonstrado estar em concordância com a expectativa com um

erro de 7.46 %. O dispositivo mostra, também, um desvio padrão do tamanho de passo médio de 23.5 %, quando o passo mínimo é usado, o que não é esperado que aconteça para tamanhos de passo superiores, como no caso de uma medição d-scan ($\sim$100 µm). Esta espectativa foi confirmada através de medidas de um laser de Titânio-Safira de 7 fs e observando que o algoritmo d-scan retorna resultados consistentes em termos de erro RMS (2 %), largura de pulso ($\sim$8.6 fs) e potência de pico ($>$95 %). O objetivo para o custo de produção de 500 € foi também atingido.

Finalmente, desenvolveu-se um espectrómetro de Índio-Gálio-Arseneto de alta resolução, na gama de comprimentos de onda do infra-vermelho próximo. Este instrumento foi ajustado até se obter uma resolução de 3 nm no espectro de um laser DPSS de 1064 nm, demonstrando um nível de sinal de $\sim$80 % da saturação a 100 µs de tempo de integração. O dispositivo foi calibrado em comprimento de onda, obtendo-se um R^2 de 0.99998 e uma gama espectral de $[950.5 - 1722.5]$nm. Foi, também, obtida a calibração do instrumento em intensidade, usando uma lâmpada de luz branca. Ao medir o espectro de uma lâmpada de vapor de Mercúrio, demonstrou-se que a resolução de 3 nm mantém-se constante ao longo de toda a gama espectral. Demonstrou-se que espectros adquiridos pelo espectrómetro desenvolvido encontram-se em concordância com os obtidos com um espectrómetro de InGaAs de referência. Os dois dispositivos demonstram resoluções da mesma ordem, sendo que o espectrómetro desenvolvido possui uma gama espectral cerca de 35 % maior do que o produto comercial. É importante notar que o dispositivo desenvolvido é extremamente compacto com um tamanho total de 120 mm $\times$ 75 mm $\times$ 47 mm. Para além disso, o custo de produção deste dispositivo foi mantido abaixo do orçamento de 3500 €.

Contents

List of Figures

List of Tables

Glossary

2DSI	Two-dimensional spectral shearing interferometry
CAD	Computer-aided design
CNC	Computer numerical control
CPA	Chirped pulse amplification
CW	Continuous wave
DPSS	Diode-pumped solid-state
DRC	Design rule check
FLIM	Fluorescence lifetime imaging microscopy
FOD	Fourth order dispersion
FROG	Frequency resolved optical gating
FWHM	Full width half maximum
GDD	Groud delay dispersion
GPIO	General-purpose input-output
KLM	Kerr-lens modelocking
LED	Light-emitting diode
LVTTL	Low-voltage TTL
MIIPS	Multiphoton intrapulse interference phase scan
NIR	Near-infrared
OP-AMP	Operational amplifier
OPL	Optical path length
PCB	Printed circuit board

RF	Resolution factor
RMS	Root-mean square
SEA-SPIDER	Spatially-encoded arrangement SPIDER
SHG	Second-harmonic generation
SPIDER	Spectral phase interferometry for direct electric-field reconstruction
TCSPC	Time-correlated single-photon counting
TOD	Third order dispersion
TTL	Transistor-transistor logic
UV-VIS	Ultra-violet to visible

Chapter 1

Introduction and Motivation

Ever since the invention of the first laser, almost 60 years ago, the technology has been applied to numerous areas in science, technology and even day-to-day life. However, lasers have come a long way from the three-level Ruby system developed by Maiman in 1960 [1]. Today, with the advent of ultrafast lasers, with pulse lengths of the order of the femtosecond (10^{-15}s) or even attosecond (10^{-18}s), lasers are at the cutting edge of scientific development in areas such as atomic, molecular and solid-state physics. Furthermore, these ultrashort pulses have many industrial applications in micro/nano-fabrication [2] and in the area of medicine [3].

To make full use of the advantages provided by such short pulses, one must correctly characterize them. For this, the d-scan technique (short for dispersion scan) invented by M. Miranda et al. [4] at the University of Porto and Lund University, and further developed by Sphere Ultrafast Photonics, allows for the correct retrieval of the pulses phase and thus characterize and optimize them both in duration and peak power. The technique achieves this by performing an indirect measure of the pulses, introducing increasing amounts of a dispersion-characterized optical glass and measuring both the fundamental and the second-harmonic generation spectrum of the pulse at each thickness step. A computer algorithm is applied to the data and the electric field of the pulse is calculated for each of the insertion steps.

This masters thesis was developed as a project in Sphere Ultrafast Photonics with the aim of achieving a low-cost adaptation of the d-scan product by custom designing some of the devices required by the technique. To do so, we aim to develop a high precision translation stage to be used in the scanning process of the technique and a near-infrared (NIR) Indium-Gallium-Arsenide (InGaAs) spectrometer to acquire the spectrum of the

light sources measured by the technique. Furthermore, we also designed custom PCBs to implement triggering capabilities on the d-scan products for synchronization with low repetition rate lasers.

The present document aims to walk the reader through the development process of those devices and is organized as follows. Chapter 2 begins by introducing the physics of ultrashort laser pulses, the technical characteristics behind their generation and how they can be controlled using the d-scan technique. Then, an overview of the technical aspects behind developing both a high precision translation stage and an InGaAs spectrometer are presented, together with an analysis of existing commercial products that fit the same purpose as those two devices. Chapter 3 goes through the design of a custom PCB to integrate the trigger feature in a d-scan product. Chapter 4 details the development of the high precision translation stage, presenting the results of using this stage in interferometric measurements and with the d-scan technique. Chapter 5 describes how an InGaAs spectrometer was designed and developed, demonstrating its use in acquiring spectra of different light sources in the near-infrared region. Finally, Chapter 6 summarizes this thesis and presents an outlook on the obtained results.

Chapter 2

State of the Art

2.1 Ultrashort Lasers

The aim of this first section of this dissertation is to introduce the reader to ultrashort pulsed lasers by going through the theoretical description of such pulses, explaining the technical characteristics that make such a pulse achievable by a laser and by discussing the application of such devices.

2.1.1 Ultrashort Pulses Description

An ultrashort pulse can be represented either in the time or spectral domain, which are related through the Fourier transform,

$$\tilde{U}(\omega) = \mathcal{F}\{U(t)\} = \int U(t)e^{-i\omega t}dt \tag{2.1}$$

$$U(t) = \mathcal{F}^{-1}\{\tilde{U}(\omega)\} = \frac{1}{2\pi}\int \tilde{U}(\omega)e^{i\omega t}d\omega \tag{2.2}$$

where,

$$\tilde{U}(\omega) = \tilde{U}^*(-\omega) \tag{2.3}$$

since $U(t)$ is a real quantity.

Furthermore, a pulse can be described by an envelope (low frequency phase variation) and a carrier (high frequency), in the time representation,

$$U(t) = \Re\{|U(t)|e^{i\phi(t)}\} = \Re\{A(t)e^{i\omega t}\} \tag{2.4}$$

where $A(t)$ is a complex quantity whose phase varies much slower than the carrier frequency [5]. Furthermore, the pulse can also be represented, in the spectral domain, by a spectral envelope and a phase,

$$\tilde{U}(\omega) = |\tilde{U}(\omega)|e^{i\phi(\omega)}. \tag{2.5}$$

This representation is of extreme usefulness when dealing with linear optics since most effects can be easily described in the frequency domain.

2.1.2 Spectral Phase

Understanding the spectral phase, $\phi(\omega)$, in Eq. 2.5 is paramount in achieving the shortest possible pulses. Since one can obtain the electric field as a function of time by Fourier transforming the spectral domain pulse (Eq. 2.2), applying a phase to the pulse in the spectral domain is equivalent to a change in the shape of the pulse in the time domain.

The spectral phase is usually described by a Taylor series expansion around a central frequency ω_0,

$$\phi(\omega) = \phi_0 + \phi_0'(\omega - \omega_0) + \frac{1}{2!}\phi_0''(\omega - \omega_0)^2 + \frac{1}{3!}\phi_0'''(\omega - \omega_0)^3 + ... \tag{2.6}$$

where ϕ_0', ϕ_0'' and ϕ_0''' are, respectivelly, the first, second and third-order partial derivatives of ϕ in respect to ω, at $\omega = \omega_0$.

The first term of the expansion, ϕ_0 represents the absolute phase of the pulse and is relevant when dealing with few-cycle pulses. The linear phase term, ϕ_0', is called the *group delay* and represents a delay of the pulse in the time domain, relative to a certain reference time. Since, often, a reference of the pulse arrival time is not available, this term is usually ignored.

Thus, even though every term of the expansion is relevant when dealing with few-cycle pulses, here we will only be interested in the expansion terms from the second order forwards, which affect the shape of the pulse by a process called *dispersion*.

2.1.3 Dispersion

In general, when a pulse is propagating through a material, the carrier and the envelope do not travel at the same velocity and neither do all the frequencies in a broad bandwidth light source - usually, longer wavelengths travel faster than shorter ones (in the frequency

band often described as having *normal* dispersion). An ultrashort laser is an example of such a light source. Thus, we need to take into account the phenomenon of dispersion in order to obtain the shortest pulses possible, since this effect leads to a reshaping (and often a stretching) of the pulse in the time domain.

The second order coefficient of Eq. 2.6, ϕ_0'', is called the *group delay dispersion* (GDD) and is the first term of the expansion to contribute to dispersion of the pulse. GDD introduced by a certain material can be estimated by computing its wavelength dependent index of diffraction, $n(\lambda)$, and taking its second-derivative at the wavelength of choice. This value can then be used to estimate the effect of a certain amount of the material on a pulse traveling through it. Particularly, one can use this information to estimate the change in pulse width. Since the effect of GDD on a broadband pulse is to effectively lag some wavelengths relative to the others, any amount of non-zero GDD that the pulse has will affect its temporal width. This becomes increasingly important the shorter the pulses due to the larger bandwidth required to generate them (see Sec. 2.1.4).

The third order coefficient, ϕ_0''', is the *third-order dispersion* (TOD) which results from the frequency dependence of the GDD and also deforms the shape of the pulse. Finally, when dealing with ultrashort pulses, with duration less than $\sim$30 fs, it is of extreme importance to compensate the dispersion introduced by not only GDD but also TOD and FOD (*fourth-order dispersion*).

2.1.3.1 Dispersion Compensation

To compensate for the dispersion phenomenon, we can use certain elements and optical configurations which introduce what is usually described as "negative" dispersion. Using these assemblies we can obtain the opposite effect to the one introduced by normal dispersion - shorter wavelengths will now travel faster than longer ones.

Gratings and Prism Compressors

The first method used to obtain negative dispersion is a grating compressor such as the one in Fig. 2.1 [6]. This technique allows for a high degree of negative dispersion to be introduced while keeping the design fairly compact. This method of compression is still widely used in chirped pulse amplification (CPA) systems, whose authors (Ref. [7]) received the 2018 Nobel Prize in Physics. However, a grating compressor is less efficient than a chirped mirror compressor (see below) [8].

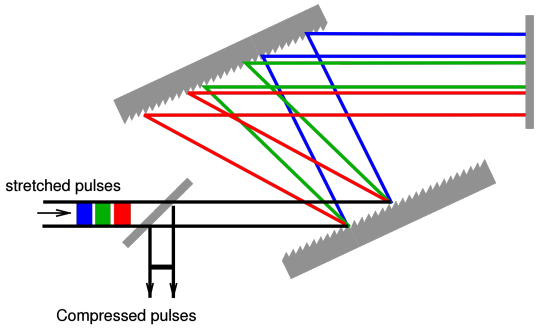

FIGURE 2.1: Double gratings compressor.

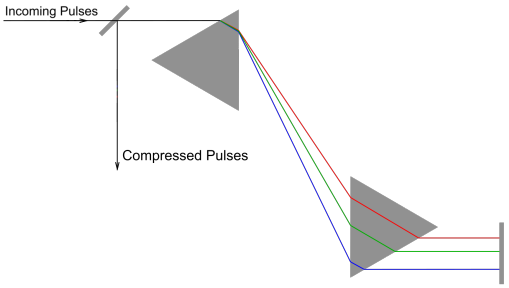

FIGURE 2.2: Double prism compressor.

Dispersion compensation can also be obtained by using a prism compressor (Fig. 2.2). This technique introduces less losses since the prisms can usually be used at Brewster angle. However, there is an intrinsic dispersion introduced by the glass in the prisms, which limits the amount of dispersion compensation achievable with the technique. Furthermore, larger distances are required between the prisms to achieve the same amount of negative dispersion as with a gratings compressor, thus the use of a prism compressor implies a loss of compactness.

Chirped Mirrors and Wedges Compressors

Another type of dispersion compensation can be obtained by the use of multilayer coatings, forming a chirped mirror [9]. These elements present a high reflectivity ($> 99.5\%$ over an 80 THz frequency range) and a nearly constant negative GDD, which can be adjusted to compensate a certain amount of a reference material (e.g. 1.5 mm of Fused Silica glass [10]). These mirrors are also usually manufactured in matched pairs which cancel each other's residual GDD oscillations.

The principle of operation of a chirped mirror is that each wavelength penetrates a different number of layers inside the mirror, thus being delayed a certain amount. In order to compensate for normal dispersion, it is desirable that longer wavelengths are delayed relative to shorter ones (Fig. 2.3). When using a pair of chirped mirrors to that effect, one must also take into account the mirrors' efficiency band which is normally limited to some hundreds of nm.

This kind of mirrors can be used in a configuration such as in Fig. 2.4 to introduce a certain amount of dispersion. The mirrors are specified to compensate for a certain amount of dispersion per bounce. Thus, the mirror pair can only introduce a discrete amount of negative dispersion which does not provide sufficient resolution to compensate

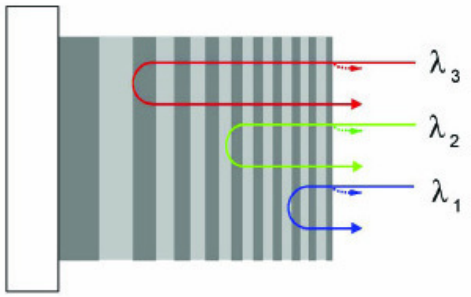

FIGURE 2.3: Chirped mirror schematic from Ref. [12]. Negative GDD is introduced if $\lambda_1 < \lambda_2 < \lambda_3$.

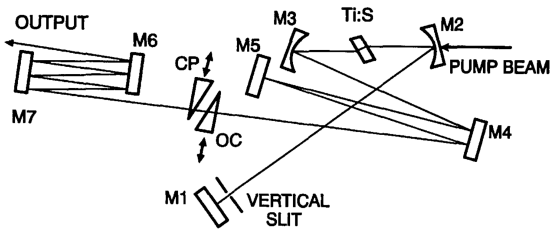

FIGURE 2.4: Chirped mirror compressor (M1, M4-M7) used in Ref. [13] to achieve 11 fs pulses from a Kerr-lens mode-locked Ti:sapphire laser.

for an arbitrary amount from a general ultrashort laser. To overcome this issue, a pair of glass wedges can be used to introduce a much smaller amount of normal dispersion on a negatively chirped pulse, thus compressing it even further. This setup introduces what is usually called a chirped mirror and glass wedges compressor which is widely used when dealing with state of the art few-cycle lasers [4] [11].

2.1.4 Ultrashort Pulses Generation

The most common lasers operate in what is called the continuous wave (CW) regime. These lasers typically emit at a very specific monochromatic wavelength, continuously in time, and can operate on one or multiple cavity modes [14] [15] [16].

On the other hand, for a laser to produce ultrashort pulses, several other conditions must be met. Firstly, such a laser requires a large gain bandwidth, which, taking into account the uncertainty principle [17], determines the so-called Fourier limited pulse with the shortest possible duration. This wide bandwidth can be achieved by using a laser medium such as Titanium-doped Sapphire, which is used in many state of the art ultrashort lasers [18] [19] [20]. However, a broad gain bandwidth alone is not sufficient in obtaining short pulses in time since, typically, such a laser will still only emit in a narrow bandwidth around the cavity mode with the highest gain. Thus, the phase of the multiple modes needs to be synchronized so that they constructively interfere and generate a well defined pulse in time.

Most modern Ti:sapphire lasers achieve this synchronization using a mechanism known as Kerr-lens mode-locking (KLM). This method takes advantage of Kerr-lensing, which occurs due to a change of the refractive index of the laser medium across the beam profile of a Gaussian beam, if there is sufficient intensity in the crystal [21]. This effect introduces

a temporary lens in the gain medium which self-focuses the laser beam. By aligning the cavity to achieve an overlap between the pulse and the pump region on the gain medium, the Kerr-lensing effect functions as a soft-aperture which introduces higher losses on the CW mode, thus making the laser favour the mode-locked regime [22].

2.2 Ultrashort Laser Pulse Characterization Techniques

In order to develop and reliably make full use of ultrashort laser pulses, it is often extremely important to characterize said pulses correctly. However, no instrument is capable of directly measuring events on the short time scale of the femtosecond or even attosecond achieved by these laser systems. Thus, indirect measurements must be performed to characterize, mainly, the duration and peak power of the pulses.

The first techniques to appear were based on nonlinear autocorrelation of the pulse. The method consists on splitting the pulse in two lines and introducing a time delay in one of them (using, for example, a Michelson interferometer setup). Then, the second harmonic of the recombined pulse is generated and its average power is measured as a function of the introduced time delay (see discussion in Ref. [23]). Although interferometric autocorrelation contains information on the pulse chirp and, consequently, bandwidth, it fails to provide information about the pulse phase and can only provide a good estimate of the temporal duration if the pulse is perfectly Gaussian.

Improvements to these measurement techniques were made in 1993 with the introduction of the frequency resolved optical gating (FROG) technique [24]. FROG expands on the interferometric autocorrelation by also employing beam splitting and time delay (thus requiring interferometric precision) and measuring not only the average power of the recombined pulse but also its frequency spectrum. Thus, we obtain a measure of the pulse spectrum as a function of the introduced time delay, which is related to the spectrogram of the pulse. From this two-dimensional plot - also called a FROG trace - the pulse intensity and phase can be retrieved through a two-dimensional phase-retrieval algorithm. Furthermore, the FROG trace itself provides additional information on the pulse, such as the length of the trace along the time delay axis providing an indication of the pulse width. On the other hand, FROG has ambiguities related to the TOD of the signal and is not able to determine if the pulse has a pre or post-pulse, which is of major importance when handling ultra-high intensity laser systems. There are also many variants of the FROG technique available such as single-shot versions which require higher pulse energy [25]

and collinear geometries that provide increased bandwidth and additional information that is helpful in validating the measurement results [26][27].

Spectral phase interferometry for direct electric-field reconstruction (SPIDER) [28] has also been developed to characterize ultrashort pulses. The technique relies on spectral shearing to overcome the intrinsic need to provide a reference to a linear interferometric measurement in order to retrieve absolute phase information. Thus, SPIDER splits the original pulse in two replicas: one which will then be further divided into another replica and delayed in time by a certain amount, τ, and one which will be chirped. These replicas are then recombined such that each of the two non-chirped replicas interfere with different, essentially monochromatic, spectral sections of the chirped replica, applying a spectral shear, Ω, to the pulses. The recombined pulse is then upconverted in a sum-frequency generation crystal and the spectral interferogram is recorded with a spectrometer. All that remains is to relate the interference fringes to the phase of the pulse, by applying a retrieval algorithm. The first step is to Fourier transform the interferogram into the time domain which will return a series with components centered at $t = 0, \pm\tau$. Then, a filter is applied to isolate only the component centered at τ. The remaining signal is inverse transformed back into the spectral domain. By taking the phase of this signal, $\theta(\omega)$ and using a calibration trace, the term associated with the delay between the two interfering replicas can then be removed. We thus obtain the relative phase difference between frequency components separated by Ω from which the phase, $\phi(\omega)$, can be obtained by integration,

$$\theta(\omega) = \phi(\omega) - \phi(\omega - \Omega). \tag{2.7}$$

It is important to notice that the SPIDER technique is highly sensitive to spectral "holes" - regions of zero spectral intensity. Specific approaches must be used to deal with those cases, such as described in Refs. [29] and [30]. The technique also intrinsically requires high spectrometer resolution in order to resolve the interference fringes. There are, however, several SPIDER based techniques that reduce the spectrometer resolution demand such as spatially-encoded arrangement SPIDER (SEA-SPIDER) [31] and two-dimensional spectral shearing interferometry (2DSI) [32].

More recently, in the early 2000s, a new technique based on phase scanning introduced a new paradigm in the area. The multiphoton intrapulse interference phase scan (MIIPS) [33] consists in applying known spectral phase curves to a pulse and using nonlinear detection to correct the original phase of the pulse. Passive elements such as gratings

or prism compressors can be used to apply the known phase curves. However, a more typical implementation of MIIPS uses a pulse shaper as the active element which controls the introduced phase. Considering an ultrashort laser pulse in the spectral domain,

$$\tilde{U}(\omega) = |\tilde{U}(\omega)|e^{i\phi(\omega)} \tag{2.8}$$

and applying a spectral phase $\varphi(\omega)$, it is straightforward to see that the SHG signal of the pulse will depend on both the original phase, $\phi(\omega)$, and the introduced phase, $\varphi(\omega)$. It can also be shown that a maximum SHG signal is obtained for a pulse with a flat phase. Thus, one can experimentally determine what introduced phase at a frequency ω maximizes the SHG signal at frequency 2ω. However, the MIIPS approach does not completely determine the original phase of the pulse in a single calculation. Because of this, one has to iteratively acquire a MIIPS trace, use the pulse shaper to compensate for the phase of the pulse and repeat this process until a flattening of the pulse phase is obtained. Besides that, the MIIPS technique is not able to retrieve the phase of the pulse when spectral holes are present.

A new technique was presented in 2011, the d-scan (short for dispersion scan) [4]. The method borrows from the MIIPS idea of performing a phase scan but uses passive elements to introduce the scanning spectral phase, instead of employing a pulse shaper.

2.2.1 d-scan

The d-scan technique [4] aims to retrieve the spectral phase of an ultrashort laser pulse making use of a chirped mirror and glass wedges compressor and a SHG crystal. Since these passive elements are already widely used in many ultrashort laser systems, the technique requires only the addition of a SHG crystal and a precise control of the wedges position. Thus, the alignment is also very straightforward since the technique does not require any beam-splitting or interferometric precision. The d-scan can also be implemented in a very compact setup and can fully retrieve the pulse phase - even when spectral holes are present -, providing valuable insight on the measured pulses.

The technique is based on the measurement of both the original pulse spectrum (or fundamental spectrum) and the second-harmonic generation spectrum corresponding to said pulse. SHG is a process in which two photons of the same frequency (and thus energy) combine to form a single photon with double the frequency (double the energy)

[34]. The second-harmonic signal is usually generated using a SHG crystal such as the one in Ref. [35].

A dispersion scan is performed by changing the dispersion of the pulse using optical glass wedges and measuring the SHG spectrum at each thickness step (also called insertion). This results in a two-dimensional trace like the one in Fig. 2.5. Here, it is important to notice that a key feature of the d-scan measurement technique is that there is a one-to-one (bijective) relation between the electric field and the d-scan trace.

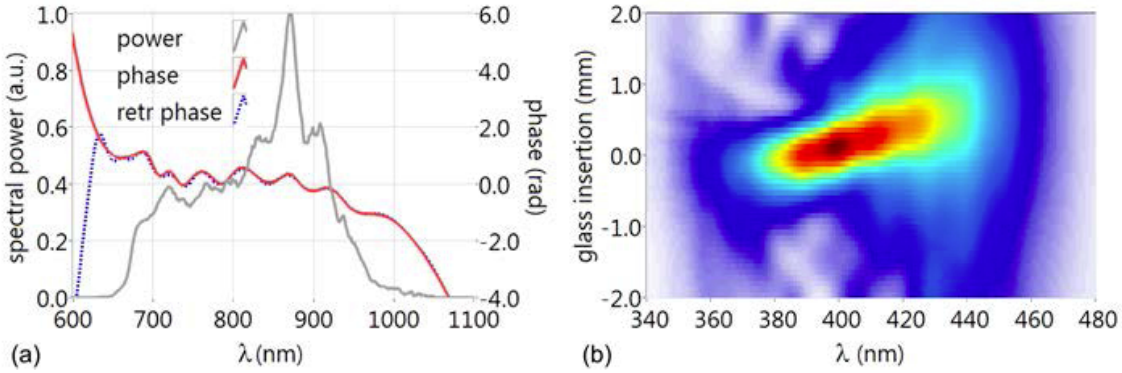

FIGURE 2.5: Typical d-scan two-dimensional trace. Simulated d-scan trace from a pulse with a phase curve consisting of third-order dispersion and phase ringing. Taken from Ref. [4].

The problem is then reduced to a two-dimensional phase retrieval one: we must find out what phase needs to be applied to the original pulse to obtain the measured second harmonic signal. This process is entirely done using a computer algorithm and, unlike the MIIPS technique, does not require iterative actuation on the pulse shape to fully retrieve its phase.

Firstly, we must compute the phase introduced at each position of the glass wedges by taking the Sellmeier formulas and the properties of the wedge glass. By taking a guess of the phase of the original pulse, defined by any set of parameters, and adding it to the one introduced by the wedges, we obtain a *guess* phase for the original pulse. From here, this guess can be applied to the measured fundamental spectrum of the beam which will then be Fourier transformed to the time domain and squared, simulating the SHG process - assuming the simple model that the SHG signal is the square of the time-dependent field. An inverse Fourier transform outputs the guess SHG spectrum of the original pulse, at each insertion step, forming the theoretical d-scan trace. Finally, an error minimization algorithm is applied which, by actuating on the parameters of the guess phase, matches

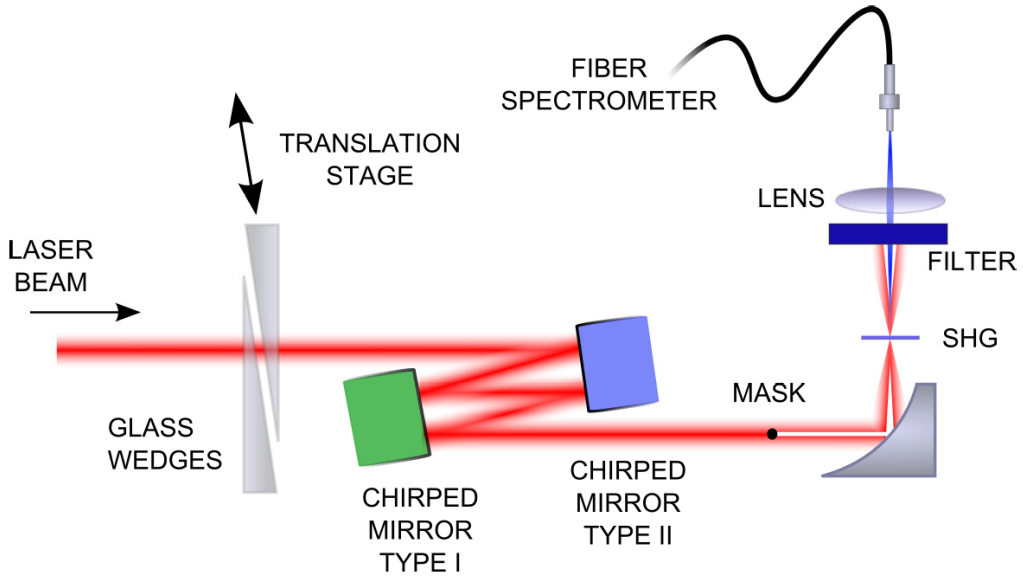

FIGURE 2.6: Typical d-scan experimental setup. Notice the translation stage for the positioning of the glass wedges and the fiber spectrometer for measuring the SHG signal. Taken from Ref. [36].

the theoretical trace to the measured one, thus fully retrieving the original phase of the pulse at each insertion step, which is used to compute the electric field of the pulse.

We, finally, obtain a two-dimensional plot of the SHG spectra of the pulse at each step of introduced glass, knowing exactly the electric field of the pulse at each insertion step and thus its pulse width and peak power. With this data, we can then choose the appropriate insertion value (i.e. ammount of dispersion introduced by the wedges) to best compress the pulse. The translation stage used to move the glass wedges can then be set to the chosen position and from that moment forward the d-scan setup is used as a passive element, optimized to compensate for pulse dispersion.

2.2.1.1 d-scan Technical Characteristics

In order to perform a d-scan measurement as explained above, some engineering considerations must be made. A typical d-scan setup is shown in Fig. 2.6.

Firstly, we can see that the glass wedges composing the compressor are moved by a translation stage which is, ideally, controlled by software on a computer. The movement of the glass wedges should preferably be as fine as possible so that small adjustments can be made to the compressor to compensate for small variations in the phase of the pulse. Thus, a state of the art translation stage should be used. Some examples of such stages are shown in a following section.

Furthermore, the technique relies on the accurate measurement of both the fundamental and SHG spectra of the light source. For this, fiber spectrometers are used due to the easy coupling of the light to the spectrometer entrance, their compactness and parallel acquisition (a full spectrum can be acquired with multiple devices at the same time). These devices are required to have enough spectral resolution to measure features of the order of the nanometre on the pulse spectrum. Such devices are commercially available and some examples will be shown further ahead.

Finally, when one wants to take a d-scan measurement of an ultrashort low repetition rate laser, a triggering of the d-scan spectrometers is required in order to synchronize the pulse emission with the spectrometers acquisition. Examples of such laser systems are present in Refs. [37] and [38], as well as in the Extreme Light Infrastructure Attosecond Light Pulse Source (ELI-ALPS) international facility which features laser sources in the TW peak power regime at repetition rates in the Hz and KHz regimes [39].

Taking all of this into account, this work is mainly incident on developing a low-cost translation stage capable of controlling the glass wedges on the compressor, on developing a low-cost compact spectrometer to be used for the acquisition of the pulse spectrum, and on integrating a triggering signal on the d-scan products.

2.2.1.2 d-scan Applications

Every since its first appearance in 2011, the d-scan technique has been used as an enabling technology for a numerous amount of applications. The technique has been successfully used with a number of different devices ranging from standard oscillators [40] to hollow-fiber compressors [41] [42].

A major emphasis of modern physics is on the generation and use of attosecond scale pulses which have been shown to have various different applications, for example in atomic, molecular, solid-state physics [43] and, more recently, XUV multidimensional spectroscopy [44]. The d-scan technique has been applied for the generation of such attosecond pulses [45].

The d-scan has also been used in the generation of relativistic electron beams driven by kHz single-cycle pulses. These electron bunches could potentially be used in applications such as ultrafast electron diffraction, ultrafast imaging and femtosecond X-ray generation [46].

Furthermore, d-scan has enabled the development of a novel multicolor bioimaging technique: SyncRGB-FLIM [47]. This technique is based on the excitation of multiple chromophores on labelled samples by a broadband few-cycle laser. By pairing this excitation with the time-correlated single-photon counting (TCSPC) technique, fluorescence lifetime imaging microscopy (FLIM) images can be obtained, thus enabling the localization of different chromophores in the cell based on their fluorescence decay properties. This process is only possible due to the powerful dispersion compensation of the microscope optical components, using the d-scan technique.

Finally, the d-scan technique can also be applied to achieve the shortest pulses possible. Recently, single-cycle pulses down to 2.2 fs have been measured by using specific strategies revolving around the d-scan technique [48].

2.3 High Precision Translation Stage

A linear translation stage is a device that enables the movement of an object in a particular direction. In the case of the d-scan technique, a translation stage is used for stepping a glass wedge which sequentially introduces a certain amount of dispersion on the laser pulse under measurement. The technique requires a high degree of control on this movement and thus a high precision translation stage must be used.

This section will introduce the main engineering aspects which must be taken into account when building such a translation stage. Furthermore, a market analysis will be performed to assess the available commercial options for this kind of product.

2.3.1 Translation Stage Technical Characteristics

In building a high precision translation stage some technical aspects need to be taken into account such as the travel range, the stepping resolution, the maximum speed, the total size of the device and the interface with the computer. Furthermore, from a business point of view, the price of the device is important and should be kept to a minimum.

In Fig. 2.7 we can see a typical glass wedge pair setup used in the d-scan technique. One of the glass wedges is typically fixed while the other is moved, by a translation stage, parallelly to the first. Eq. 2.9 can be used to compute the insertion length of glass, Δy, for a certain translation stage step, Δx, and a glass wedge of angle θ.

$$\Delta y = \Delta x \cdot sin(\theta) \tag{2.9}$$

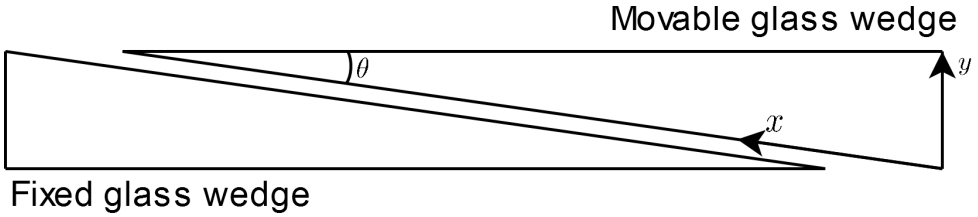

FIGURE 2.7: Diagram of the glass wedges pair typically used in a d-scan system. The translation stage moves the wedge in the x direction. The insertion value per step of the translation stage is dependent on the angle of the wedges, θ.

The first parameter to account for is the travel range of the stage which should be enough to allow for the full range of insertion values. This corresponds to the length of the glass wedge used which varies with both the total amount of dispersion that the compressor is designed to compensate and the required resolution of the dispersion steps, Δy_{min}, which is dependent on the angle, θ, of the glass wedges. Furthermore, when choosing the travel range of the translation stage, one must also account for the required minimum insertion value and the beam size which greatly increases the necessary travel range.

This brings us to the next characteristic of a translation stage, the minimum step resolution. As mentioned in [4], Sec. 3, a typical value for the angle of the glass wedges is 8 ° which allows for a stage step length of over 100 µm for very fine thickness steps of 20 µm. Note that these translation steps are more than three orders of magnitude larger than the allowed by state of the art translation stages, which provide a minimum step length of less than 100 nm. Thus, we can conclude that such a stage is possibly an overkill for the majority of applications of the d-scan technique, only becoming useful when the pulse changes very rapidly with dispersion and thus a high resolution thickness step is required.

Furthermore, the maximum stepping speed of the translation stage is an important factor when performing a dispersion scan since, from a client point of view, the faster the measurement of the pulse is performed, the better. The speed of a high precision stage varies from the tens to the hundreds of millimetres per second.

For the integration of the translation stage in a compact product to be used in many different scenarios, the size of the overall device is rather important. Even though this parameter is mainly limited by the travel range, it can be optimized by keeping the protrusion of the controller and interface cables, to a minimum.

The communication interface of the translation stage is also important from a compatibility and compactness point of view. Generally, commercial stages either communicate with a computer via *RS-232*, *USB* or *Ethernet*. Here, a trade-off between standardization, speed and implementation difficulty must be considered when choosing between the three interfaces.

Finally, from the point of view of the production of a d-scan system, the price of the translation stage must be considered. Since most commercial stages present higher capabilities than required by the technique (mainly resolution-wise), these devices are, intrinsically, expensive. Thus, we expect that a much cheaper alternative can be custom developed to more adequately fit the needs of a d-scan product.

2.3.2 Market Analysis

When considering the development of a custom made alternative to any product, it is important to study the existing commercial choices. This allows us to set design goals and to have perspective on how such a product is usually built.

For this study, the selected products all have a 50 mm travel range so that a basis of comparison can be established. These devices were compared in terms of stepping resolution, maximum speed, overall size, the implemented communication interface and price. As seen above, these parameters are all relevant for the integration of such a device in a d-scan product. Results for this comparison are summarized in Table 2.1.

The first commercial translation stage studied is a top-of-the-line product in terms of minimum step resolution, supporting step lengths of less than 50 nm (Stage #1 in the table). However, this high resolution comes with a sacrifice in maximum speed which is limited to 7 mm/s in this device. The same manufacturer also produces a lower resolution alternative to this model: Stage #2. The minimum step length of less than 0.2 µm on this alternative is still much better than the required by the d-scan technique. These larger steps allow the stage to have a higher maximum speed of 29 mm/s. Furthermore, these two stages are both controlled with an *RS-232* interface which can be adapted to a *USB* connection. Even though these devices also present a rather small footprint, they are among the most expensive products available.

Stage #3 is, again, a high resolution product with minimum steps of 0.125 µm. However, this is a much slower alternative to the previous models supporting maximum speeds of 1.2 mm/s. This is still a compact stage, with a footprint comparable to the

other models. This device communicates with the controlling computer via the *RS-232* protocol. This stage is also priced above the ideal budget.

Stage #4 offers a 0.5 µm maximum step resolution and more compact than the previously studied ones. However, the main advantage of this stage is its high speed of 500 mm/s which is possible due to it being a servo motor driven stage instead of the typical stepper motor used in the other alternatives. Although this is a great feature for many other applications, this is not needed for a d-scan product since the scanning speed would still be limited by the integration time of the spectrometers. On the other hand, this stage allows for the connection to be established through a *USB* connection, albeit only through the external controller required to drive the stage. Besides that, this product is rather expensive to be used as an OEM part. This manufacturer also offers a higher resolution (0.05 µm), lower speed (2.4 mm/s) translation stage, Stage #5. This device again has to be externally controlled and uses *USB* for the computer interface. This stage also features a lower price than the other one.

The last two stages set a reference for a different motion technology: the piezo electronics. This technology can be advantageous in resolution, repeatability and compactness but it is hard to implement as a custom product. Stage #6 provides a stepping resolution of $\sim$1 nm, much less than the other mentioned products, while keeping the maximum speed rather high at 20 mm/s. The main adavantage of this stage is its high compactness relative to the servo or stepper motor ones. Stage #7 also provides a high stepping resolution, 0.025 to 1.25 µm, together with a high maximum speed, 200 mm/s, and compactness. However, both of these stages require an external controller which is usually larger than the ones used by a traditional stage, which require less electronics. This reduces the overall compactness of piezo stages. The price for both these products is approximately the same, sitting around the middle of the price range established by the other devices.

Stage #	Resolution (µm)	Maximum Speed (mm/s)	Size (mm)	Communication Interface	Price
1	0.0476	7	172.9 x 65.0 x 21.0	*RS-232 / USB*	€€€€
2	0.1905	29	172.9 x 65.0 x 21.0	*RS-232 / USB*	€€€€
3	0.1250	1.2	180.0 x 62.0 x 42.0	*RS-232*	€€€€
4	0.5000	500	145.0 x 57.0 x 35.0	*USB*	€€€€
5	0.0500	2.4	160.8 x 43.0 x 22.0	*USB*	€€
6	0.0010	20	80.0 x 17.0 x 8.5	*USB*	€€€
7	0.0250 - 1.2500	200	50.0 x 34.0 x 13.0	*USB*	€€€

TABLE 2.1: Market analysis for high resolution linear translation stages.

2.4 Spectrometers

A spectrometer is a device capable of measuring the light intensity as a function of the emitting wavelengths of a source. The produced measurement is called the spectrum of the source.

The light entering a spectrometer, typically passes through four optical components before the spectrum is acquired. First, the incident light passes through an entrance slit which forms an interference pattern in a cone of light and ultimately helps to improve the resolution of the device. The cone of light is then incident on a spherical mirror which collimates the beam. The diffraction grating then splits the beam in its several wavelengths by reflecting them at different angles, according to,

$$sin(\theta_m) = sin(\theta_i) - \frac{m\lambda}{d} \tag{2.10}$$

where d is the spacing between the grooves of the grating and m is the order of the reflection. The angles θ_i and θ_m can be understood by observing Fig. 2.8 and are, respectivelly, the incident angle of the beam and the reflected angle of the respective wavelength λ on order m of the grating. It is important to note the relation between the orders of the grating and the wavelengths of the source. If wavelength λ is reflected by an angle θ for order $m = 2$ of the grating, then wavelength 2λ will be reflected at the same angle, θ, at order $m = 1$ of the grating. This relation will later be exploited during the alignment of

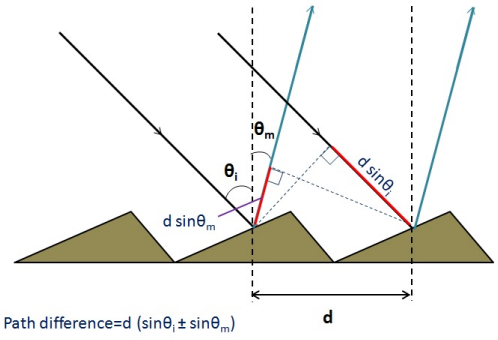

FIGURE 2.8: Diffraction grating reflection of a ray incident with angle θ_i.

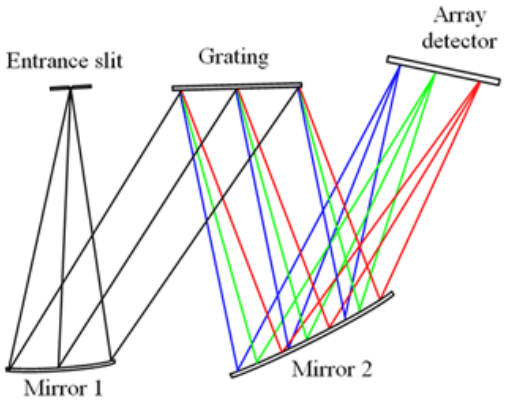

FIGURE 2.9: Typical Czerny-Turner spectrometer geometry.

the spectrometer. Finally, the light leaving the diffraction grating is incident on a second mirror which focuses the beam of light on the detector.

An example typical configuration of a spectrometer is the Czerny-Turner one shown in Fig. 2.9. Even though this geometry is very effective when building a spectrometer, it is not the most compact since one is limited by the size and focal distances of the mirrors. Thus, as will be shown later, in this work the collimating mirror will be replaced by a parabola in order to make the geometry more compact.

2.4.1 Spectrometer Technical Characteristics

When selecting a spectrometer for a specific use, several technical characteristics have to be taken into account. Here, we will focus on the most important ones for the d-scan technique and for establishing a comparison between several state of the art spectrometers.

The first characteristic is the resolution of the device. In order to accurately measure the spectrum of a light source, the spectrometer must be able to resolve features smaller than the smallest feature of the source (e.g. smaller than 10 nm if the light source has a peak of 10 nm in linewidth). This implies that the application must be taken into account when choosing the resolution of the spectrometer.

In the development of a spectrometer, one must take into account several factors which impact resolution such as the slit width (W_s), the groove density of the diffraction grating ($1/d$) - which impacts the wavelength range ($\Delta\lambda$) of the device -, the number of pixels on the detector (N_p) and the width of each pixel (W_p). The spectral resolution ($\delta\lambda$) can thus be estimated using Eq. 2.11 [49].

$$\delta\lambda = RF\frac{\Delta\lambda \times W_s}{N_p \times W_p} \tag{2.11}$$

Note that, in this equation, a resolution factor (RF) is introduced because the spectral resolution is measured at the full width half maximum (FWHM) of the peaks. Since we need to take at least 3 pixels to measure the FWHM of a peak, $RF = 3$ when $W_s \sim W_p$. The resolution factor is smaller for smaller values of the pixel width until it stabilizes at $RF = 1.5$ when $W_s > 4W_p$.

Moreover, in order to compare this theoretical resolution to the actual resolution of the device, a light source of sufficiently narrow resolution must be chosen. If the light source peaks are wider than the spectrometer resolution, no conclusion can be made about the latter since the resolution of the acquired spectrum is limited by the linewidth of the source [49].

Furthermore, when designing a spectrometer one must consider the existent trade-offs when trying to improve resolution. First, resolution improves with a higher groove density on the diffraction grating, since we are effectively reducing the spectral range of the device (see Eq. 2.11). Second, resolution can be improved by a smaller width entrance slit but at the expense of signal strength, since the amount of light that enters the spectrometer is reduced [50]. Due to these trade-offs, a specification of the spectral resolution of a spectrometer is only valid when coupled with a definition of the spectral range and signal strength of the device.

Thus, another main requirement for the development of a spectrometer is the spectral range, which is perhaps the most important one since it impacts the light sources which can be measured with the device. As seen above, the spectral range greatly impacts the resolution of the device and thus should be carefully selected to reflect the application of the spectrometer. In order to measure the entire spectrum of certain light sources of large bandwidth (e.g. ultrashort lasers) a spectral range of the order of several hundreds of nanometers is required [51].

We must then take into account several factors which impact the spectral range of the spectrometer. We can readily see from Eq. 2.10 that the groove density (d) of the diffraction grating is one of those factors, since a higher groove density will result in the wavelengths of the light source to be spread across a wider angle. This results in a smaller range of wavelengths hitting the focusing mirror - and, subsequently, the detector - if the rest of the spectrometer geometry remains unchanged.

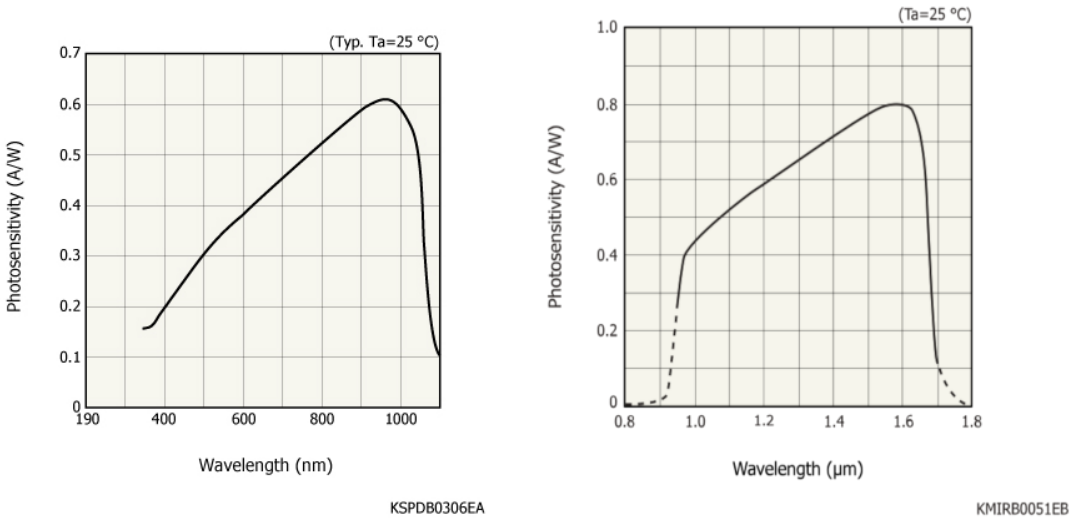

FIGURE 2.10: Detectors spectral response. Left: Si photodiode [52]. Right: InGaAs line detector [53].

Furthermore, so that we may take full advantage of the spectral range of the light that reaches the detector of the spectrometer, this component must be carefully chosen. For a common, ultra-violet to visible (UV-VIS) spectrometer, a silicon (Si) detector can be used, since its response only falls off at $\sim$1100 nm (see Fig. 2.10, left). However, when we wish to acquire spectra on the near-infrared (NIR) wavelength range, an indium gallium arsenide (InGaAs) detector must be used, since the spectral response of this material goes from $\sim$900 nm to $\sim$1700 nm (Fig. 2.10, right).

An estimation of the spectral range of the device can be obtained by performing ray-tracing simulations, in the design phase, or by calibrating the spectrometer in terms of wavelength, after the assembly of the device. The spectral range of the device can be adjusted to fit a specific desired window, by, for example, changing the incident angle of the beam on the diffraction grating, thus changing the output angle of the diffracted rays (see Eq. 2.10).

In the context of the d-scan technique, multiple spectrometers have to be used in order to simultaneously acquire the SHG and linear spectra of the source (see Sec. 2.2.1). Besides that, those two steps of the technique require the spectrometers to have different spectral ranges since the SHG effectively doubles the frequency of the linear spectrum. However, a common feature between the spectrometers used in the technique is the high resolution, in order to minimize the error introduced in the computation, by the acquisition of the spectra. Since the project resources only allow for the development of one prototype

spectrometer, we chose to develop a NIR, high resolution one, whose requirements reflect the needs of the d-scan technique.

2.4.2 Market Analysis

So that we may better understand the required characteristics of the spectrometer we want to develop, we must look into the state of the art of near-infrared spectrometry. To do so, we analysed five different devices which were compared in terms of spectral resolution, spectral range, size and price. The result of this comparison is compiled in Table 2.2.

Spectrometer #1 is the smallest among the devices under analysis, which makes it a suitable candidate to allow an easy integration in a product. This device also has a spectral range of $[950 - 1650]$nm, which is around the desired $[900 - 1700]$nm for an NIR spectrometer. However, the 10 nm resolution is not sufficient for the application in mind. This reduced resolution is a result of the high compactness and the use of a sensor with a small number of pixels. Even though the technical characteristics of the device are not sufficient for the application in mind, its price is within the acceptable range.

Spectrometer #2 fits the application needs both in terms of spectral range - $[900 - 1700]$ nm - and resolution - 3.1 nm. However, the improved spectral range and resolution are a result of a larger footprint than the previously considered device, which makes this an unsuitable candidate for compact product integration. This device is a high resolution and high sensitivity spectrometer with a price over 10 000 €, suitable for other applications.

Spectrometer #3 features a higher resolution than any of the other considered - 1.5 nm. However, this resolution is a result of both a smaller spectral range - either $[900 - 1300]$nm or $[1200 - 1600]$nm - and a larger footprint than any of the other devices. Thus, this spectrometer is much better suited for laboratory work than for a product integration application also due to its price of over 10 000 €.

Spectrometer #4 has a spectral resolution of $3 - 12$nm, which depends on the choice of spectral range and entrance slit. The spectral range of the device can be chosen to be any range of wavelengths between 900 nm and 1700 nm, allowing for an improvement in resolution. Furthermore, this device has the smallest footprint among the considered 3 nm resolution spectrometers. By featuring all of these important characteristics, this spectrometer is a suitable device to easily integrate in a product. Moreover, this device is also a good candidate in terms of price.

Finally, Spectrometer #5 features a maximum wavelength range of $[1000 - 1750]$nm and a resolution of $2 - 50$nm, which again depends on the chosen entrance slit and spectral range. It is also a rather compact product with a footprint not much larger than device #4. Besides that, this spectrometer fits the budget for such a device and is thus a good option to fill this role.

Spectrometer #	Spectral Resolution (nm)	Spectral Range (nm)	Size (mm)	Price
1	10	950-1650	89.1 x 63.3 x 31.9	€€€
2	3.1	900-1700	182.0 x 110.0 x 47.0	€€€€
3	1.5	900-1300 / 1200-1600	198.1 x 109.2 x 68.6	€€€€
4	3-12	900-1700	70.5 x 104.0 x 42.0	€€€
5	2-50	1000-1750	100 x 130 x 40	€€€

TABLE 2.2: Market analysis for NIR high resolution spectrometers.

Chapter 3

Trigger PCB

3.1 Introduction

In this chapter we will detail the development of a printed circuit board (PCB) for the external triggering of multiple instruments required for the d-scan technique. This external triggering is fundamental when working with low repetition rate lasers, so that the d-scan spectrometers are synchronized with the ultrashort pulses.

In developing this PCB, we began by setting the requirements for the board so that it fulfils the needs of a d-scan product both in terms of the devices that require triggering and taking ease of integration into account.

We then created a set of design guidelines to obtain the best results during the manufacturing process of the boards. The design process was then performed, following these guidelines. Here, we developed the several electrical circuits implemented on the board.

Finally, after the manufacturing of the boards, the results were evaluated in terms of the fulfilment of the set requirements and by assessing the product integration process.

3.2 Requirements Analysis

We began the development of the PCB with the definition of the requirements that fulfil the triggering needs of a d-scan product.

The first requirement for the PCB is the conversion from the power input of the d-scan device - 12 V or 15 V - to 5 V to be used in the powering of the PCB and any other instrument that requires it.

The main input of the PCB is the external trigger signal. For this, the PCB should use a coaxial connector of the *Hirose U.FL* type [54], which connects to a coaxial cable input that provides the external Transistor-Transistor Logic (TTL) signal.

This trigger signal will be provided by the laser source with which we would like to synchronize the d-scan instruments. Thus, the PCB must support input signals at the repetion rates of the lasers which are in the ranges of 0.1 Hz to 10 Hz from ultra-high energy lasers in the PW regime [55], 1 kHz to 3 kHz from CPA systems [46] or 100 kHz to 300 kHz from fiber laser systems [56]. Thus we specify that the maximum delay from the input to the output signal should be in the order of 1 µs so that all of these repetition rate ranges can be used with the PCB.

The trigger signal must then be opto-isolated to protect from voltage spikes and transients, avoid ground loops and impedance mismatches, which could damage or interfere with the acquisition of the instruments. To achieve this isolation, a circuit based on an opto-coupler should be used.

Furthermore, the PCB must convert the TTL signal input to a Low-Voltage TTL (LVTTL) level to be used with devices which require this signal level.

The PCB should also implement an electronic circuit capable of driving a light-emitting diode (LED). This circuit will use a General-Purpose Input/Output (GPIO) pin from a spectrometer to control the On/Off status of the LED. This light source will be used in the d-scan product for the intensity calibration of the spectrometers.

The complete PCB - including all the electrical components and connectors - should also be compact enough to facilitate its integration inside a commercial product. Thus, its outer dimensions should not exceed 50 mm $\times$ 60 mm $\times$ 6 mm.

The product integration should also be made possible by the use of at least two M3 mounting holes on the board.

Finally, if possible, the PCB should allow for the interface with multiple GPIO pins on the instruments under control for debugging and development purposes.

The requirements set for the trigger PCB are available in the following table and in Appendix A.

#	Requirement	Description	Priority
1	Power Conversion	Implement a DC-DC converter capable of converting a 12 V or 15 V input to 5 V.	Mandatory
2	Trigger Input	Implement a TTL trigger signal input using a *Hirose U.FL* coaxial connector.	Mandatory
3	Timing Delay	The PCB should introduce a maximum delay of 1 µs on the trigger signal.	Mandatory
4	Opto-isolation	Implement a circuit based on an opto-coupler to isolate the input trigger signal from the instruments under control.	Mandatory
5	Signal Conversion	Convert the TTL signal to Low-Voltage TTL (LVTTL).	Mandatory
6	LED Driver	Implement an LED driver for the intensity calibration of spectrometers in a d-scan product.	Mandatory
7	Size	Achieve dimensions of less than 50 mm × 60 mm × 6 mm for the component populated board.	Mandatory
8	Mounting Holes	Implement at least two M3 mounting holes for securing the PCB to the product	Mandatory
9	GPIO Pin Interface	Implement an interface with the GPIO pins on the instruments under control.	Desired

TABLE 3.1: Technical requirements for the development of a trigger PCB.

3.3 Design

The developed PCBs were designed to meet the requirements, using a set of rules compiled for this purpose. The Eagle Computer-aided Design (CAD) software was used to design the electrical circuits and the physical layout of the boards.

3.3.1 PCB Manufacturing Checklist

In order to make the designed PCBs ready for manufacturing, a set of rules was developed based on the SparkFun Eagle Design Rules [57] and on common aspects that arose during the development of these PCBs. These rules were then compiled into a checklist

which was used at each iteration of the PCBs design.

The checklist is divided as follows:

- Components - e.g. check footprint, check orientation;
- Layout - e.g. via and trace size;
- Dimensions - e.g. hole and pads size tolerances;
- Silkscreen - e.g. readable in one or two directions, helps with populating the board;
- General - e.g. use SparkFun.dru for Design Rule Check (DRC) instead of Eagle's predefined DRC.

3.3.2 Electrical Circuit Design

In order to fulfil the requirements set above, four main electronic circuits were implemented on the PCB: a trigger input circuit, an opto-isolation circuit, a TTL to LVTTL voltage converter and a LED driver circuit.

The trigger input circuit (Fig. 3.1) consists of the *Hirose U.FL* connector as the input connector, a 5 V Zener diode to limit the input voltage, a general purpose diode for current inversion protection of the circuit and a 300 Ω resistor. This last element serves as a current limiter for the signal input pin of the opto-coupler that follows the trigger input circuit.

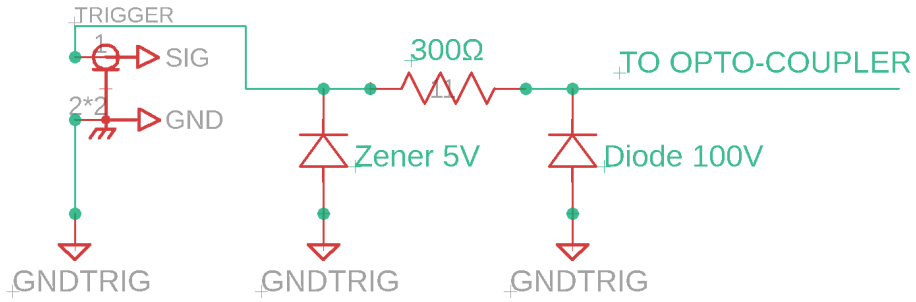

FIGURE 3.1: Electronic circuit for the input of the TTL trigger signal.

The second circuit present in the PCB implements the opto-isolation of the trigger signal (Fig. 3.2). This circuit consists of an opto-coupler and an inverting buffer. The opto-coupler is an IC that uses a micro-led and photo-diode pair to electronically isolate the input and output signals. By letting the input trigger signal drive the LED in the IC, the original signal can be retrieved on the photo-diode on the output of the IC. However, by specification of the opto-coupler IC used in this circuit, its output signal is inverted

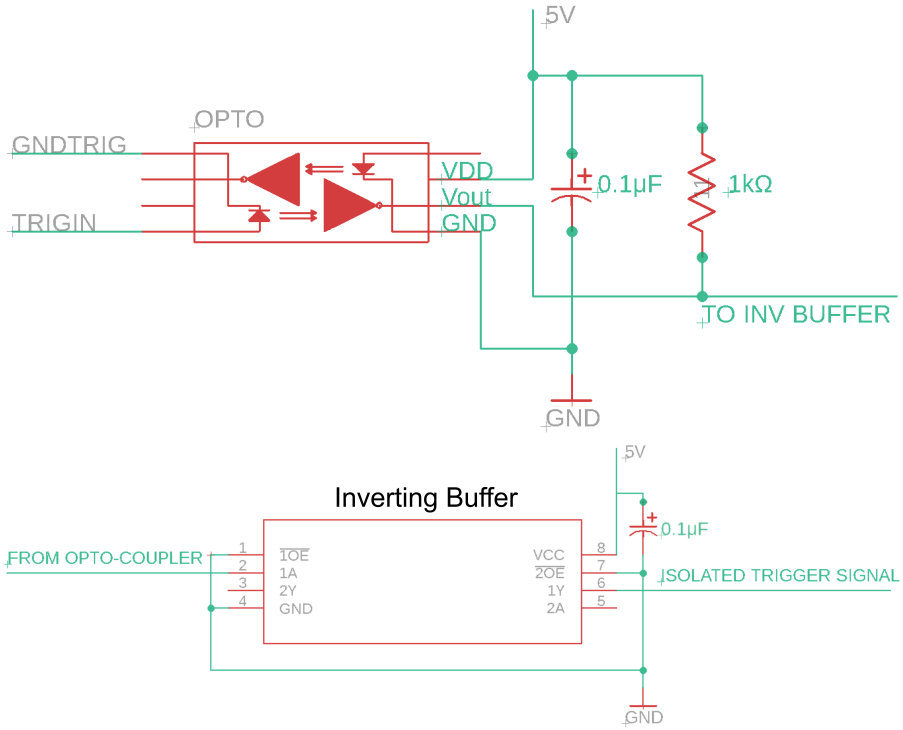

FIGURE 3.2: Electronic circuit for the opto-isolation of the trigger signal.

relative to the input. Besides that, the IC provides a low output current, thus an inverting buffer is required to obtain a final isolated trigger signal of the same polarity as the overall input one and with sufficient current to drive the trigger pins on the instruments. Furthermore, since most of the electronic delay will be introduced by the opto-coupler IC, we chose a device specified for maximum delays of 100 ns, in order to fulfil the specified timing requirement of 1 µs. Finally, it should be noted that each of the two integrated circuits is powered through a decoupling capacitor of 0.1 µF, as required by the previously established PCB design guidelines.

To complement the opto-isolation circuit, a TTL to LVTTL voltage converter was implemented to allow for the control of devices that take the lower voltage levels as input. This circuit is a simple voltage divider, using the 3.6 V Zener diode as a voltage limiter. According to Eqs. 3.1 - 3.4, any TTL signal that enters this circuit at a voltage level between $[0-5]$V is converted to a LVTTL signal with between $[0-3.3]$V if the appropriate resistor ratio, R_2/R_1, is chosen so that, when the input signal is high (5 V), $V_2 \sim 0.3$ V and, thus, $V_{LVTTL} \sim 3.3$ V.

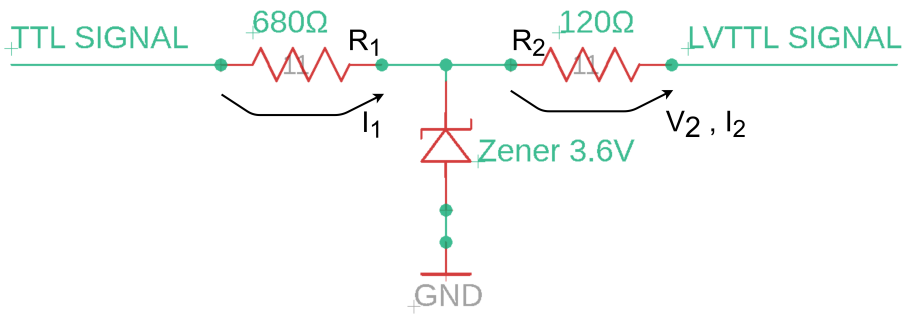

FIGURE 3.3: Electronic circuit for the TTL to LVTTL conversion of the trigger signal.

$$I_1 = \frac{V_{TTL} - V_{Zener}}{R_1} = \frac{1.4}{R_1} \tag{3.1}$$

$$I_2 \sim I_1 \tag{3.2}$$

$$V_2 = I_2 \cdot R_2 = 1.4 \cdot \frac{R_2}{R_1} \tag{3.3}$$

$$V_{LVTTL} = V_{Zener} - V_2 = 3.6 - V_2 \tag{3.4}$$

Finally, the PCB is required to allow the control of a LED with a GPIO pin from an instrument. To achieve that, a driver circuit was implemented by using a NPN transistor with a base current limiter resistor and a LED current limiter resistor, R_c, calculated following Eq. 3.5, where I_c is the collector current on the transistor, which should be limited according to the LED specifications.

$$R_c = \frac{V_{cc} - V_{LED} - V_{CE}}{I_c} \tag{3.5}$$

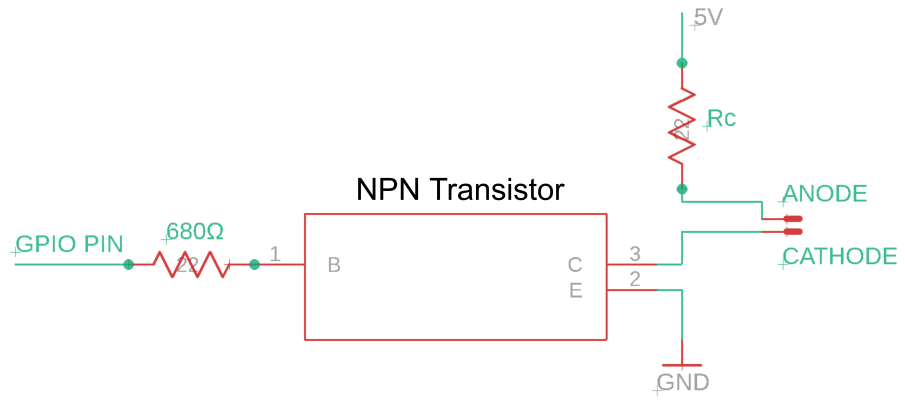

FIGURE 3.4: Electronic circuit for the LED driver controlled with a GPIO pin.

3.3.3 Design Results

The final product of the PCB design phase is shown in Figs. 3.5 and 3.6. Here, two different PCB designs are presented. PCB a) on Fig. 3.5 follows all the required specifications, including both the TTL to LVTTL and LED driver circuits. PCB b), on Fig. 3.6, on the other hand, does not implement these two circuits, since there was a need for a more compact version of the PCB which implements only the trigger isolation circuit.

Furthermore, a design choice was made to use a commercially available board for the power conversion circuit. This external board is electronically connected to the designed PCB through four single headers and using two mounting holes for extra mechanical robustness.

We can also immediately see from the figures that the external dimensions of the boards are well within the set requirement thus making them ideal for a compact application.

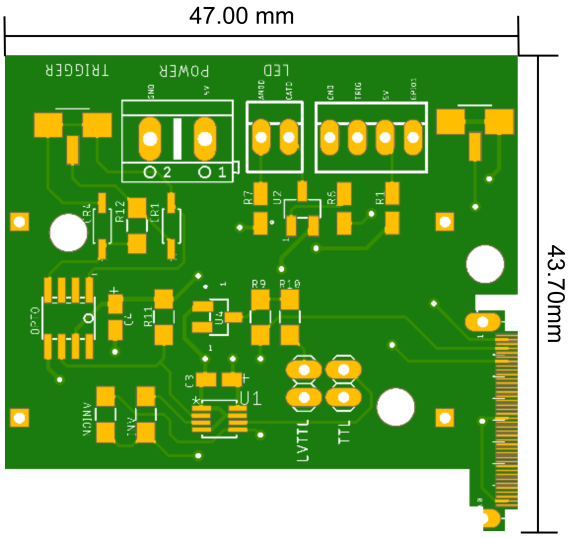

FIGURE 3.5: Design result for PCB a).

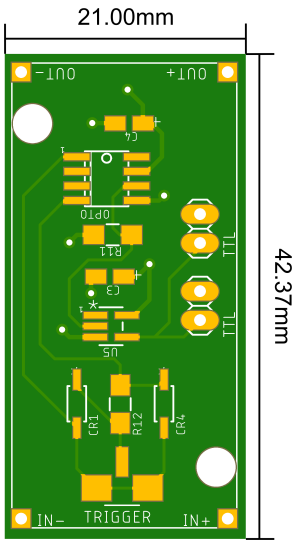

FIGURE 3.6: Design result for PCB b).

3.4 Results

The successful design of the developed PCBs will be characterized by their fulfilment of the set requirements and by the ease of the integration of the PCBs on a product.

3.4.1 Requirements Fulfilment

By following Table 3.1, we can evaluate the fulfilment of the set requirements for the designed triggering PCB.

The first requirement is the DC-DC conversion between 12 V or 15 V to 5 V. This requirement was met by using a commercially available PCB, externally connected to the design PCB by individual headers and mounting points for extra mechanical security.

Furthermore, the trigger signal input was readily implemented using a *Hirose U.FL* connector, on the designed PCB, as required. The circuit was tested at trigger repetition frequencies from 0.1 Hz up to 1 MHz, which fulfils the specified requirements.

This input trigger signal was then opto-isolated using a dedicated IC and the isolated signal was level converted from TTL to LVTTL, in order to be used as an external triggering signal to different devices. Thus the main requirements for the board were fulfilled and the developed PCB can be used for its main purpose.

Moreover, an LED driver circuit was shown to be working to control an LED with a GPIO pin from a connected device. The GPIO pins interface was also implemented, for debugging reasons.

Finally, both of the developed boards were kept under the set requirement for size, as can be seen in Figs. 3.5 and 3.6, and can thus be integrated in a compact product.

#	Requirement	Achieved
1	Power Conversion	Yes. Using external DC-DC converter.
2	Trigger Input	Yes.
3	Timing Delay	Yes. Tested for range [0.1Hz - 1MHz].
4	Opto-isolation	Yes.
5	Signal Conversion	Yes.
6	LED Driver	Yes.
7	Size	Yes.
8	Mounting Holes	Yes.
9	GPIO Pin Interface	Yes.

TABLE 3.2: Fulfilment of the set requirements for the development of a trigger PCB.

3.4.2 Product Integration

The final step in the development of the PCBs was the product integration. The boards were designed with that purpose in mind, by leaving easily accessible mounting holes for spacers and screws, to secure the boards to the casing of the product. It was necessary, however, to adjust the design of this casing to the placement of the mounting holes and to allow for sufficient slack to account for the cables on the PCB.

The product integration of the PCBs is thus easily achieved by simply connecting all the trigger signal cables (e.g. input and outputs) and mounting the boards using the mounting holes. This integration has already been achieved with success in a number of d-scan products.

3.5 Chapter Review

In order to perform the external triggering of multiple devices used in a d-scan product, a trigger PCB was developed as part of this project.

We began by setting the requirements for the PCB, taking into account the aim of integrating the PCB in the product. The most important requirements for the PCB are the implementation of a circuit capable of optically isolating the input trigger signal from the signal sent to the devices under control, the implementation of a signal conversion circuit from a TTL power level to a LVTTL one and the control of a LED using a GPIO pin from one of the instruments.

We then moved on to designing the PCB using a CAD software. For that, a set of PCB design guidelines was compiled to make sure that the final design product was ready for manufacturing. The electrical circuits implemented on the board are discussed here. To conclude the design section, the results are presented in the form of two different PCBs, one with all the implemented circuits and one which only isolates the trigger signal without converting it to LVTTL or having LED control capabilities.

Finally, the PCB development is evaluated in terms of the fulfilment of the set requirements and the ease of product integration of the board. We conclude that all the requirements were fulfilled and that the board is adequate for a product integration since it requires only the attachment of the external power PCB, the connection of the input and output trigger cables and the placement of mounting screws to secure the board to

the product casing and thus guarantee its physical integrity. This integration has already been successfully achieved in several d-scan products.

Chapter 4

High Precision Translation Stage

4.1 Introduction

In this chapter, we will explain the development process of a high precision translation stage to be used with the d-scan technique.

We will begin by setting the requirements for the device in order to make sure that the final prototype can be used effectively with the technique and is close to the industry standard established in the state of the art analysis.

Then, we will move on to detailing the design of the translation stage. Here, we will define the architecture of the device, explaining the design of the custom computer numerical control (CNC) manufactured parts required to build the stage and of the control PCB as well as the design.

Furthermore, the prototype assembly process will be detailed with the alignment of the stage with the DC stepper motor and the correct positioning of the glass wedges.

Finally, we will explain the experimental procedures that have allowed us to perform both an interferometry measurement of a CW laser and a d-scan of an ultrashort laser, using the developed translation stage. The results from these experiments will be presented and analysed. These results will be used to assess whether the set requirements were fulfilled.

4.2 Requirements Analysis

The requirements for the high precision translation stage will be set taking into account the needs of the d-scan technique and the state of the art research previously performed.

A summary of this analysis is available in Table 4.1 and in Appendix A.

Firstly, as previously mentioned, the device is not required to have such a high resolution as some of the examples from state of the art stages, due to its particular application to the d-scan technique. Thus, the developed translation stage should achieve a minimum step length of at least 100 µm.

Furthermore, it is important to set a requirement for the travel range of the device. A typical value for this parameter is 50 mm, which is the value used to establish a comparison between the several state of the art stages and is thus the set requirement.

Besides that, the translation stage should perform a d-scan with a relatively fast stepping speed. Thus, a requirement is set to have the stage achieve a maximum speed of 20 mm/s which is typical among the researched market products.

The developed device should also be compact so that it can be easily integrated in a d-scan product. Thus, the overall size of the translation stage should not exceed 180.0 mm $\times$ 70.0 mm $\times$ 30.0 mm. Since this stage is also meant to have an integrated controller and support the direct application of glass wedges both to its base and to the moving platform (see below), this product should end up being more compact than the available market alternatives.

Furthermore, the device should allow for the communication to be established through a standard *USB* connection. A *C++* library should also be available to control the stage via software.

Due to its particular application, the stage should support the use of glass wedges of 5° and 10°, which means having metric optical table mounting holes at these particular angles.

Furthermore, the stage should also support the calibration of a *home* position. This sensor will be used by the controller to establish a reference for the position of the platform, when the stage is first powered up.

The assembly should also include a manual control knob so that one is able to move the platform without having to control it via the *USB* connection. This knob should allow the movement to be made in any direction and control the speed of the platform for either fast or controlled stepping.

Finally, to be desirable as an OEM product, the total cost of the translation stage, including the controller, should be kept under 500 €.

#	Requirement	Description	Priority
1	Resolution	Achieve a minimum step length of 100 µm.	Mandatory
2	Travel Range	Support a travel range of at least 50 mm.	Mandatory
3	Maximum Speed	Achieve a maximum stepping speed of 20 mm/s.	Mandatory
4	Size	Achieve a total footprint of less than 185.0 mm $\times$ 75.0 mm.	Mandatory
5	Communication Interface	Support communication with a computer through a *USB* connection and a *C++* library.	Mandatory
6	Optical Table Support	Support use with metric optical tables, at the glass wedge angles of 5 ° and 10 °.	Mandatory
7	Glass Wedge Support	Integrate the mounting of the glass wedges directly on the stage base and moving platform.	Mandatory
8	Home Calibration	Support *home* position calibration.	Mandatory
9	Manual Control	Support the use of a knob as a manual control of the movement of the stage, when power is connected.	Mandatory
10	Price	Keep the total cost of the device, including the controller, under 500 €.	Desirable

TABLE 4.1: Technical requirements for the development of a high precision translation stage.

4.3 Design

The design phase of the developed high precision translation stage begins with the clear definition of the architecture of the device. This architecture can then be used as a basis for the design of custom CNC parts to integrate in the product such as a base for placing the moving stage, the glass wedge mounts and a motor mount. Finally, the control PCB was designed, much like the triggering PCBs, with the help of Eagle CAD and following the previously compiled design checklist.

4.3.1 Architecture Definition

The architecture definition of the custom translation stage must answer all basic functional questions regarding the device.

Firstly, we must define how the stage movement will be performed. For simplicity reasons, we decided to use a classic stepper motor and screw configuration. For this, we had the option of custom designing the whole platform, which implied custom designing a lot of parts and thus impacting the overall cost of the finished product. Instead, we chose to look for a commercial alternative for the moving platform, which can be coupled to a motor capable of driving it. We chose a product that can be converted from a manual stage to a motor driven one, provided we can couple the screw to an external motor. At this point, it was important to select both the travel range and the screw lead of the platform. The platform chosen features a 65 mm travel range and a screw lead of 0.8 mm/rev, which allows us to fulfil the requirements of the product both in terms of travel range ($\geq$50 mm) and in resolution (minimum steps of $\leq$100 µm), provided the motor allows for at least eight steps per revolution.

The next step is to choose the appropriate motor for such a stage. Since the application in mind does not require a high degree of torque due to the relatively low weight loads that will be used, a compact stepper motor will be used. This motor has a stepping angle of 1.8 º (corresponding to 200 steps/rev) and has a bipolar configuration in which each phase draws a current of 600 mA. This motor can be controlled by a bipolar motor driver such as the A4988 [58] which will be integrated in the control PCB of the stage. For the coupling of the motor to the manual stage, a flexible shaft coupler will be used for its simplicity, compactness and, most importantly, misalignment compensation (e.g. [59] with a 3 º angular misalignment capability).

The control of the motor will be performed, as mentioned, using an A4988 IC, which will be paired with an Arduino Nano [60] to serve as a computer interface through a USB connection. This motor controller allows for micro-steps down to $1/16^{th}$ of a motor step (corresponding to 3200 steps/rev of the motor and a minimum step length of 250 nm for the chosen stage screw). The Arduino Nano will also implement the low-level control of the stage, driving the potentiometer knob for manual control of the stage and a linear Hall-effect sensor [61] for home position calibration of the stage. All of these control capabilities will be implemented in a compact PCB.

All that remains now is to design the physical interface between all the parts. Here, solutions must be developed to fix the stage, motor, control PCB and wedges in a convenient and compact manner. For this, custom CNC parts will be manufactured. We will go into detail on this in the following section.

4.3.2 CNC Part Design

The development of the custom translation stage required the design of CNC parts which help make the stage more compact, easy to assemble and facilitate integration in a product. Here, parts have been designed to fix the moving platform, the stepper motor, the glass wedges and the control PCB. A base has also been designed to place all the components together in order to arrive at a convenient single mechanical assembly.

A schematic of this assembly can be seen in Fig. 4.1. Here, we can see the placement of the moving platform which is attached to the base through four M4 screws. A custom designed motor holder is attached to the base by two M3 screws and secures the motor through four M2 screws. The motor is connected to the ball screw of the manual stage through the coupler mentioned above. The control PCB is also conveniently secured to the base of the stage. Two custom mounts were designed to hold the glass wedges using nylon tip M4 screws. One of these mounts is attached to the base part in the shown position, holding the fixed wedge, while the other is placed on the moving platform. Finally, we can see the M6 holes on the base which will be useful when fixing the stage to an optical table. To fulfil the requirement for compatibility with 5° or 10° glass wedges the stage must be placed on the optical table at the same angle so that the moving wedge is displaced perpendicular to the incidence of the laser beam. For this, the bottom hole acts as a pivot while the other two serve as a choice for the different angle of the wedges. These holes are also placed on a 25 mm grid for compatibility with a metric optical table. Finally, the whole base of the assembly determines the total footprint of the device as $186.3\,\text{mm} \times 74.4\,\text{mm}$.

Furthermore, the CNC parts designed to mount the glass wedges on the translation stage can be seen in Figs. 4.2 and 4.3. These mounts secure the wedges using nylon tip M4 screws which attach from the top of the CNC parts. They can then be secured either to the moving platform of the stage (Fig. 4.2) or the base of the assembly (Fig. 4.3), by normal M4 screws. In the design of these parts it was important to take into consideration the height of the moving platform relative to the base of the stage, since it is required that the

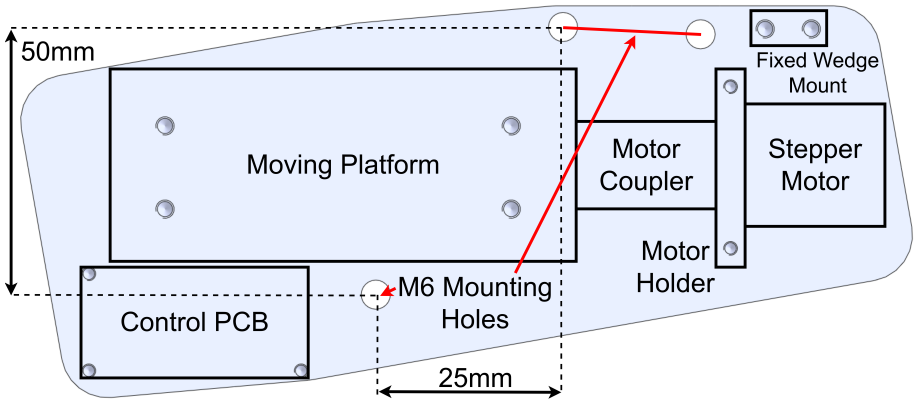

FIGURE 4.1: CNC part design for the base of the translation stage. The positions of the several components of the stage are marked on the image.

two glass wedges are at the same height, after they are mounted on the translation stage. Besides that, the mount for the movable wedge was designed with the intricate shape shown in the figure so that it able to go over the motor coupler and holder thus enabling the use of the full travel range of the device.

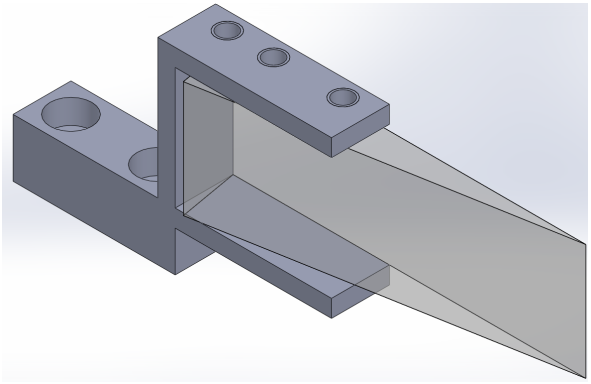

FIGURE 4.2: CNC part design to hold the movable glass wedge.

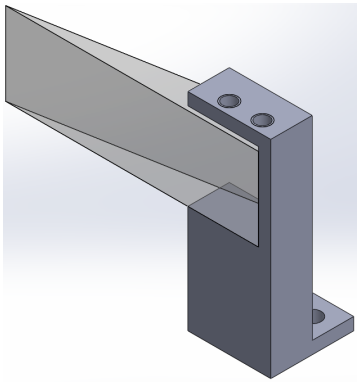

FIGURE 4.3: CNC part design to hold the fixed glass wedge.

4.3.3 PCB Design

In order to incorporate all the electronic hardware required to control the stage and implement the required features, a custom PCB was designed. Following the previously established rules for the design of a manufacturable PCB, we obtained the layout shown in Fig. 4.4.

In designing the PCB, it was important to integrate the Arduino, the A4988 controller board and interfaces for the motor, *home* position sensor and manual knob.

As per the design rules mentioned above, the motor power input is driven through a decoupling capacitor, this time of 100 µF, due to the higher power.

The manual knob is implemented using a potentiometer, powered by the Arduino and directly connected to one of its GPIO pins. By measuring the signal on this pin, one can linearly vary the translation speed of the stage, via the Arduino.

On the other hand, the linear Hall sensor used for calibrating the *home* position of the stage, is read through a more complicated electrical circuit. This consists of a voltage comparator such as the one in Fig. 4.5. The circuit uses an operational amplifier (OP-AMP) to compare the voltage levels from the Hall sensor and a voltage divider controlled by a trimmer potentiometer. While the platform of the stage, which holds a small magnet, approaches the Hall sensor, its output voltage varies linearly. When this voltage reaches a level higher than the one provided by the voltage divider, the OP-AMP switches and a signal is sent to the GPIO pin on the Arduino. The trimmer potentiometer enables the control of the position on which the triggering of the OP-AMP occurs, thus setting the reference point for the *home* position of the stage.

Furthermore, the final designed board should be as compact as possible, thus both sides were used to place components. The PCB was designed so that the Arduino should be placed from the bottom, with the *USB* connection on the right side of Fig. 4.4. The motor controller and all other components should be placed from the top.

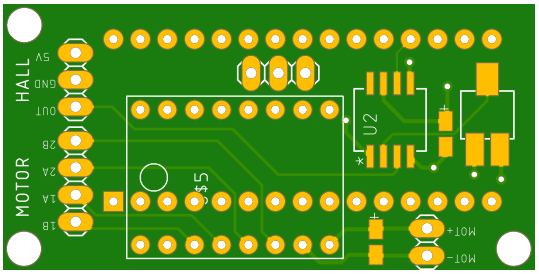

FIGURE 4.4: Control PCB for the custom translation stage.

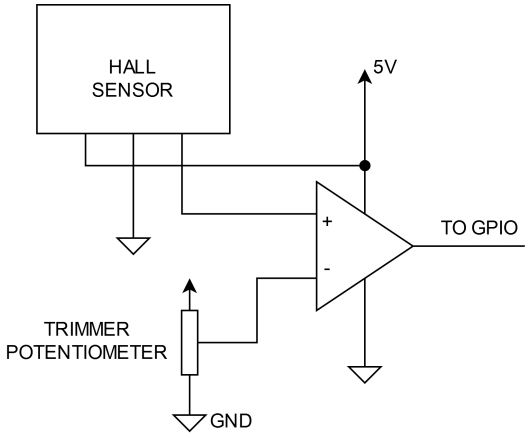

FIGURE 4.5: Voltage comparator circuit for the reading of the linear Hall sensor.

4.4 Prototype Assembly

In this section we will provide a step-by-step overview of the assembly of the developed custom translation stage prototype.

The first step in the assembly is to place the manual stage on the base with the corresponding M4 screws. At this point, no screws should be tightly secured since the ball screw of the stage must later be aligned with the vein of the motor.

Then, the motor holder should be attached to the base of the stage using the two fixing points. The motor coupler can now be attached to the motor and this assembly placed in its corresponding place, connecting the motor to the holder and the coupler to the manual stage ball screw.

At this point, an alignment of the motor with the manual stage must be performed by connecting the control PCB and turning the motor at a slow speed to watch how the rotation of the motor is being translated to the moving platform. If the coupler oscillates in any direction, an adjustment must be performed in the relative positions of the motor, motor holder and manual stage. This is critical in minimizing oscillations during any measurement that uses the stage. After performing this alignment, all the screws should be tightly secured so that the assembly is fixed.

The control PCB can now be secured to the base of the stage, using the three M3 mounting holes with adequate spacers so that the Arduino controller is not touching the base of the stage. Here, the home sensor must be positioned on the manual stage, on the opposite end from the motor, being careful to leave the correct side of the sensor facing the moving platform, since this is a directional sensor. A small $5\,\text{mm} \times 5\,\text{mm} \times 2\,\text{mm}$ magnet must be glued to the side of the moving platform to trigger the hall sensor.

Finally, the glass wedges can be placed on the assembly. In doing this, the wedges should be placed on the mounts using a flat surface so that the face of the wedges is parallel to the mounts. The wedges should be tightly secured to the mounts using the nylon tip screws to minimize their movement during displacement. When placing the wedge assemblies on the stage, they should be first roughly tightened - respectively to the moving platform and the base of the stage - so that they can later be aligned to be parallel to each other, allowing the beam to leave the wedge pair in the same direction as it enters.

4.5 Control Software

As mentioned above, the developed translation stage is controlled by an Arduino Nano, capable of interfacing with the motor controller, the manual knob potentiometer and the

Hall sensor. In this section, we will go into detail on how this control was achieved, in terms of software.

The software developed to control the translation stage is divided in two main blocks: the Arduino code and the *C++* library. The Arduino is coded to perform the most basic functions of the stage, by providing a low-level interface with the motor and sensors. On the other hand, the *C++* library implements the functions necessary to integrate the device in a product.

The Arduino code implements the functions listed below:

`void SetResolution(int N_div);`

Sets the resolution of the stage in *N_div* subdivisions of the motor step.

`void SetDirection(bool Dir);`

Sets the direction of the movement of the stage.

`void Step(int N_steps);`

Moves the stage in the defined direction and with the defined resolution, *N_steps* number of steps.

`void Home(void);`

Moves the stage to the *home* position by continuously reading the signal from the Hall sensor comparator circuit while moving the stage in the *home* direction.

On the side of the computer, the *C++* library establishes *USB* communication with the Arduino and sends commands to execute the functions shown above.

Besides that, the library implements the counting of the steps of the stage. It does this by first performing a *home* calibration of the stage, setting the step position to zero. The library then assumes that the stage travels the correct number of steps sent through the stepping command to the Arduino and updates a variable accordingly. By using the stored position of the stage, the library also implements a function to move the stage to a specified, absolute, position anywhere in the travel range.

However, this approach has the disadvantage of not accounting for the missed steps that sometimes occur during the travel of the stage but is accurate enough for the purpose

in mind. If one desires to more carefully track the position of the stage, an encoder should be added to the design, in the future.

Finally, by taking the developed *C++* library and adjusting it to fit the existing d-scan software, we achieved an interface capable of controlling the custom stage through the d-scan software. The developed code was tested by using the d-scan software not only to perform the d-scan measurements of a 7 fs ultrafast oscillator but also to acquire the data during the interferometric measurements.

4.6 Experimental Setups

This section will focus on detailing the experimental setups used to characterize the developed prototype of a custom translation stage. To do this, two setups were used: a michelson interferometer and a typical d-scan.

4.6.1 Michelson Interferometer

We began by using a Michelson interferometer setup. This kind of experiment allows for the characterization of the step length of the translation stage. A classical Michelson interferometer consists of a beam splitter which divides the incident light into two arms making a 90° angle. Each of these arms ends on a plane mirror which reflect the light back through the arm. The two beams are then made to coincide and thus interfere, forming circular fringes. Fig. 4.6 represents such a setup.

The interference pattern is typically changed by actuating on one of the mirrors, changing the effective distance one of the split beams has to travel, relative to the other. The interference pattern is highly coupled to this difference in distance between the two arms of the interferometer. The phase difference, $\Delta\phi$, between two waves is dependent on their wavenumber, k, and on the optical path length (OPL) difference between them, ΔOPL (Eq. 4.1). The maximums of the interference pattern occur for constructive interference (when the waves are in phase) and thus for differences in OPL of integer multiples of the wavelength of the light, $\Delta OPL = m\lambda$ (Eq. 4.3). Since the OPL difference in the interferometer is achieved in reflection, the maximums of this interference pattern actually occur at intervals of $\lambda/2$.

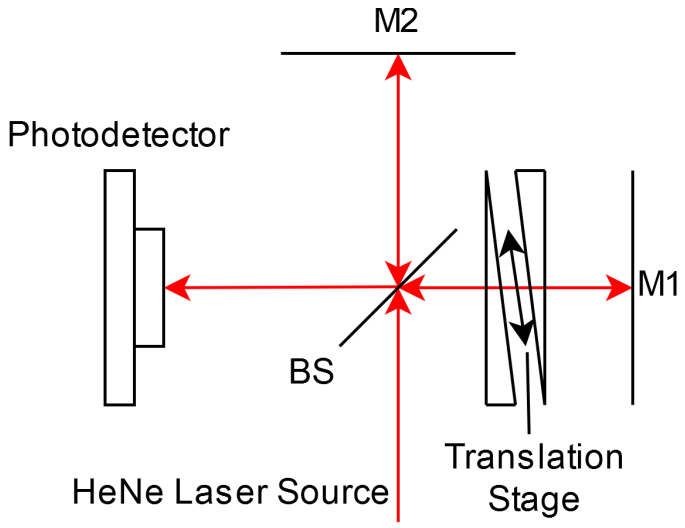

FIGURE 4.6: Michelson interferometer setup for the testing of the translation stage resolution. A HeNe laser beam is split by a beamsplitter (BS) to the two arms of the interferometer, hitting mirrors M1 and M2. By controlling the thickness of glass in the path of the beam in one of the arms, the optical path length along that arm is changed, altering the interference pattern of the two waves.

$$\Delta\phi = k\Delta OPL = \frac{2\pi}{\lambda}\Delta OPL \tag{4.1}$$

$$\Delta\phi_{max} = 2m\pi, m = 0, \pm1, \pm2, ... \tag{4.2}$$

$$\Delta OPL = m\lambda \tag{4.3}$$

However, in order to sample the interference pattern with enough points to allow for the characterization of the translation stage step size, it is important to perform several of these steps between each maximum of the pattern. A helium-neon (HeNe) laser (λ =632.8 nm) will be used as the light source for the interferometer, corresponding to an *OPL* difference between maximums of 316.4 nm. Thus, if the translation stage was used to actuate on the position of one of the mirrors on the interferometer, not even two data points could be acquired between maximums of the interference pattern, taking into account the 250 nm minimum step length of the stage.

Instead, a glass wedge pair is used to achieve OPL steps of less than the step length of the stage. Following Eq. 2.9, we can see that, using glass wedges of $\theta = 10\,^{\circ}$, a movement of the translation stage in the x direction, in the minimum step length allowed, $\Delta x =$ 250 nm, corresponds to an insertion value of $\Delta y \approx 43$ nm. The difference in refractive indexes between air and the glass of the wedges (fused-silica) must be taken into account

and thus the resulting optical path length difference is $\Delta OPL = (n_{FS} - n_{air}) \cdot \Delta y \approx 20\,\text{nm}$ for each step of the stage.

4.6.2 d-scan Setup

The second experimental setup used to test the stage is the direct application of the device in the d-scan technique as the translation stage in Fig. 2.6. This experiment will be used to characterize how the phase retrieval algorithm supports the use of the custom translation stage. This aims to test the viability of using the device in a future d-scan product.

4.7 Results

In this section, we will elaborate on the results obtained from the two experimental setups mentioned above. We will begin by analysing the data from the Michelson interferometry experiment. Then, some d-scan measurements will be performed so that the device can be evaluated directly in the application for which it was designed.

Finally, we will also analyse the fulfilment of the set requirements, thus having a figure of merit to conclude on the effectiveness of the development process.

4.7.1 Michelson Interferometer

The Michelson interferometry experiment was conducted by repeatedly moving the custom translation stage carrying the fused-silica glass wedge and measuring the intensity of the interference pattern at each step. This provides us with a plot of interference intensities vs step number of the stage. If the stepping of the stage is perfectly performed, this plot should be close to a sinusoidal function with maxima at well defined intervals. The number of steps between these maxima is directly proportional to the size of each step thus providing a measure of the actual step length of the stage.

In Fig. 4.7 we can see the plot of the number of points between each maximum for such a scan of the interferometer measure. In the figure, we have also plotted lines for the mean and one standard deviations from the mean value. By taking the mean value of 17 steps and using the relation established above, we can see that this number of steps corresponds to a variation in optical path length of $\Delta OPL = 340\,\text{nm}$. For a HeNe interferometer of this type, the maxima should occur at an OPL distance of 316.4 nm ($\lambda/2$). Thus,

the average number of steps between each maxima in the interference pattern resulting from the experiment agrees with the expectation with an error of only 7.46 %.

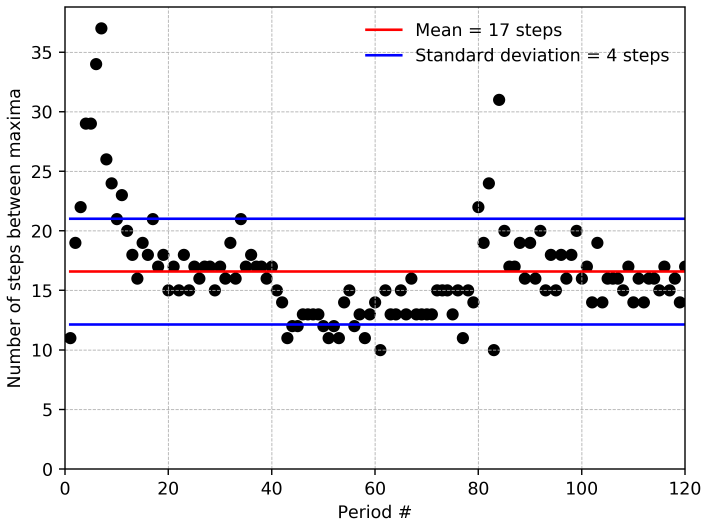

FIGURE 4.7: Number of stage steps between each maximum of the interference pattern of the Michelson interferometer. Notice the mean number of steps between each maximum, 17 steps and that most points are within one standard deviation (4 steps, in this case) from the mean.

Furthermore, the standard deviation of 4 steps from the average 17 steps indicates that the step length could potentially vary 23.5 % over a distance of ∼4 µm (17 steps times the step length of 250 nm). If this is true over the usual step lengths used for d-scan measurements (≥100 µm), this instability could pose a threat to the developed stage being used with the technique. However, the instability does not usually translate over to larger step lengths since the movement is more continuous for longer distances. This observation is common in state of the art translation stages. Finally, this experiment also reveals an initial error of the step size - shown by the first peak in Fig. 4.7 - possibly associated with a mechanical imperfection of the stage, but which was not further investigated since the achieved performance was sufficient for use with d-scan systems.

4.7.2 d-scan

The d-scan measurements made with the custom translation stage aimed to evaluate the capability of the device functioning properly in a d-scan application. Thus, it was important to assess if the d-scan algorithm was capable of accurately retrieving the phase

of the pulse, when a scan was made with the custom stage. For this, several scans of a Ti:Sapphire oscillator were performed. Fig. 4.8 shows one of the scans performed.

We can immediately see from the figure that the retrieval algorithm behaves rather well when the scan is performed with this stage, reaching a root-mean square (RMS) error of 1.8 %. This is to be expected since we know from previous experience that the algorithm is robust when it comes to oscillations in the step size [62]. Furthermore, these scans were made along a 6 mm scan range, with 128 steps, equally spaced at a step length of 46.875 µm. As mentioned above, the stage is expected to be more stable at these step lengths much larger than the minimum one.

In order to have a statistical analysis of the behaviour of the stage, several scans were performed in the same characteristics as the one in Fig. 4.8. These scans resulted in an average RMS error of 2 % for the phase retrieval and a constant pulse width of 8.58 fs with an average peak power of over 95 %.

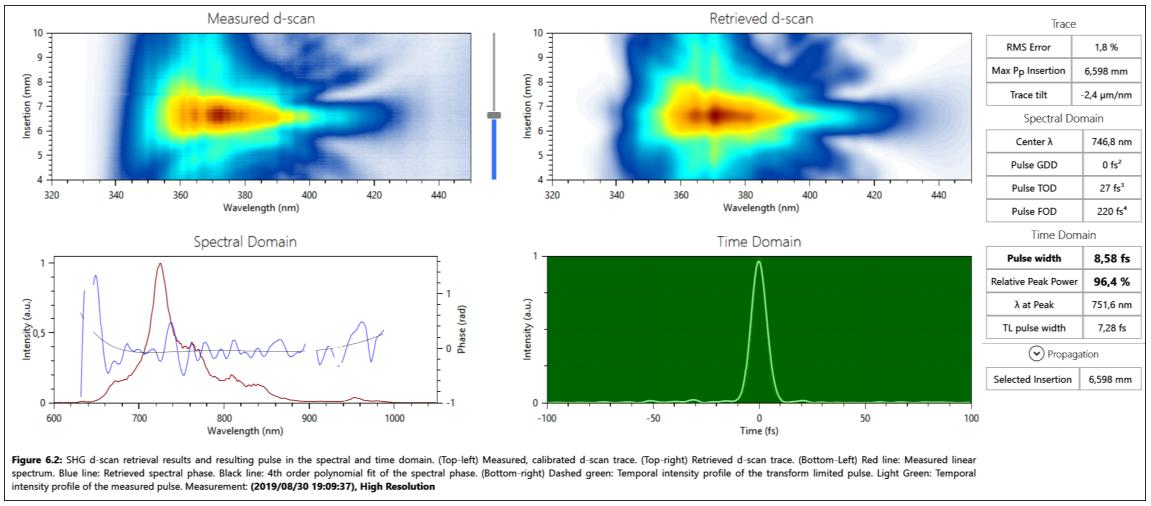

FIGURE 4.8: Result of performing a d-scan measurement with the developed translation stage.

These results show consistency of the translation stage during multiple scans and thus indicate that it would be feasible to include the developed device in a d-scan product, provided more robustness tests are applied to the stage. Such a test would be to run the stage for several hours, in a back and forth motion and then performing another set of d-scan measurements. This would allow us to conclude on the repeatability of the stepping mechanism after being used for a long time. It would also provide us a measure of the lifetime of the device in terms of travelled kilometres, a common specification given by translation stage manufacturers.

4.7.3 Requirements Fulfilment

The evaluation of the fulfilment of the set requirements is paramount in determining whether the developed device will be able to perform the functions for which it was designed.

The first set requirement for the custom translation stage was to achieve a minimum step length of 100 µm. As confirmed by the Michelson interferometer experiment, the minimum step length of the stage is close to the 250 nm limit from the choice of ball screw and motor controller, which allows us to verify the fulfilment of this requirement.

Furthermore, the selection of a manual stage with a travel range of 65 mm, as a component of the developed motorized stage allows us to achieve a larger travel range than the specified 50 mm.

Even though the maximum speed of the stage was not directly measured, since the set requirement can only be achieved in a continuous stepping mode and only stepping scans were performed (small steps intrinsically take more time due to stopping/starting the stage). Future work can be perform to verify the requirement set in terms of maximum speed of the stage.

The developed translation stage features a footprint of 186.3 mm $\times$ 74.4 mm, which is within an acceptable margin from the specifications since the glass wedges for a d-scan application can be directly mounted in this space.

Communication was established with the stage using the specified *USB* connection. A *C++* library was built to control all the features of the stage (e.g. stepping, setting resolution, *home* calibration) via a computer. This library was also adapted to support integration in the d-scan software.

Furthermore, the total assembly of the translation stage can be mounted on a metric optical table at the angles of 5 ^{o} and 10 ^{o}. By designing custom mounts, we also achieved the integration of the glass wedges directly on the stage, thus providing an ease of integration advantage when compared to stage of the art translation stages built for general purposes.

A *home* calibration sensor was integrated in the stage to define a reference point to be used when tracking its position. A knob potentiometer was implemented as a means of manually moving the stage in any direction and with controllable speed, without the use of a computer.

Finally, the total cost of the developed translation stage is below the set threshold of 500 € which makes this device a more cost-effective alternative to the market available products.

#	Requirement	Achieved	State of the Art
1	Resolution	Yes. ∼250 nm.	47 nm. Overdefined for this particular application.
2	Travel Range	Yes. 65 mm.	50 mm.
3	Maximum Speed	Acceptable for the application. Not quantified.	7 mm/s.
4	Size	Yes, within an acceptable margin. 186.3 mm × 74.4 mm.	172.9 mm × 65.0 mm.
5	Communication Interface	Yes. *USB*.	*RS-232 / USB.*
6	Optical Table Support	Yes. At 5° and 10° angles.	No direct support for mounting at a custom angle.
7	Glass Wedge Support	Yes. Direct integration.	Requires additional custom parts.
8	Home Calibration	Yes.	Yes.
9	Manual Control	Yes.	Yes.
10	Price	Yes. <500 €.	More than 3x as much.

TABLE 4.2: Fulfilment of set requirements for the development of a high precision translation stage.

4.8 Chapter Review

In Chapter 4 we detailed the development of a custom high precision translation stage fitting the need of the d-scan technique.

Firstly, we compiled a detailed list of requirements for the device which served as an essential starting point for the design of the product. These requirements later served as a figure of merit to characterize the device.

We then moved on to designing the translation stage. We began by clearly defining the architecture of the product taking into account the set requirements in the choice

of components. A manual translation stage with a travel range of 65 mm and a screw lead of 0.8 mm/rev was adopted together with a bipolar stepper motor which provides 200 steps/rev. These two components are coupled by a flexible shaft coupler which compensates for misalignment of 3° between the two components. Here, we also established that the control of the stage would be performed using an A4988 IC, capable of dividing the step of the motor down to $1/16^{th}$ of a full step and an Arduino Nano which will be the interface between the motor controller, a *home* calibration Hall sensor, a potentiometer knob for manual control of the stage and the computer which connects to the device.

Then, we provide an overview of the design of custom CNC parts to be used in the translation stage. We show how all the components of the product are compactly mounted on a base capable of being mounted to a metric optical table. This assembly also supports the direct use of 5° and 10° glass wedges for the d-scan application, through custom designed mounts.

During the design phase we also developed a PCB which fits all the electronic components required for the driving of the motor and sensors in a compact board. Here, a voltage comparator circuit was designed to serve the purpose of setting the *home* position of the stage, together with a Hall sensor.

We then moved on to detailing how all the parts should be put together during the assembly of the product. We provide step-by-step instructions on the mounting of the manual stage, the stepper motor, the coupler which connects the two, the control PCB and, finally, the glass wedges.

In order to correctly function with a computer interface, control software has been developed in the form of Arduino code and a C++ library. We show what low-level functions the Arduino code implements to control the stage and provide insight on the function of the C++ library that would later be adapted to work with the existing d-scan software.

Furthermore, we detailed to experimental setup used to perform an interferometric measure of the minimum step size of the stage. A HeNe laser Michelson interferometer was assembled. However, instead of coupling the translation stage to one of the mirrors, we took advantage of a glass wedge pair, perpendicular to the beam on one of the arms of the spectrometer, to reduce the change in optical path length of the light, when the stepping of the stage is performed. This helps us in acquiring multiple data points between each maxima of the interference pattern since, when using the minimum step length of the stage, 250 nm, we are effectively changing the OPL in steps of $\Delta OPL \approx 20$ nm. On the

other hand, a typical d-scan setup was implemented in order to test the robustness of the developed stage in performing a dispersion scan.

The results of these two experiments are then presented. The Michelson interferometer measurement allowed us to conclude that each maximum of the interference pattern occurs at an average distance of 17 steps which corresponds to a variation in *OPL* of 340 nm. We can see that this corresponds to a 7.46 % error, by taking into account the wavelength of the HeNe laser ($\lambda = 632.4\,\text{nm}$) and because the maxima are expected to occur at a distance of $\lambda/2$. Moreover, this measurement provides a standard deviation from the mean of 4 steps. This is a rather large 23.5 % deviation and could potentially be a problem when using larger step lengths, such as in the d-scan technique. However, this instability is common in state of the art translation stage and is not expected to translate to larger step values.

D-scan measurements were also performed with the custom translation stage, providing insight into the feasibility of using the device with the technique. The several performed scans provided an average RMS error of 2 % for the phase retrieval algorithm and all showed a pulse width of around 8.58 fs and a pulse peak power of over 95 %. These results are promising in the sense that they show consistency throughout scans. However, more testing should be performed in the future, mainly in determining the physical robustness of the developed stage and in measuring the expected lifetime of the product.

Finally, we evaluated the fulfilment of the set requirements for the custom product. We can say that all the requirements have been fulfilled with the exception of the maximum translation speed which was not directly measured but is expected to be within the specifications.

Chapter 5

High Resolution InGaAs Spectrometer

5.1 Introduction

Here, we will look in detail into the InGaAs, high resolution prototype spectrometer, developed as part of this project.

We will begin by defining the requirements for the device taking into consideration both the current state of the art for this kind of spectrometer and the needs of the d-scan application.

Afterwards, we will explain the design process of the prototype, walking the reader through the chosen geometry of the device, the ray tracing simulations used to define the positions of the different optical elements and, finally, through the design of custom optical mounts.

Furthermore, a table-top demonstrator was assembled in order to verify the geometry and concept of the device.

The resulting prototype will then be detailed. We will first show how the device was assembled, explaining the experimental setup used to tune, calibrate and assess the performance of the device. We will conclude by presenting some spectra of different light sources acquired with the device, establishing a comparison between the developed prototype and a state of the art product.

5.2 Requirements Analysis

The development process of the InGaAs spectrometer began with the clear definition of the requirements of the device. This definition was based on the current state of the art for spectrometer of similar characteristics and on the d-scan application needs. The result of the requirement analysis is shown in Table 5.1 and in Appendix A.

The first requirement set for the spectrometer is the spectral range, which is, perhaps the most important feature of the device. We define that the wavelength range should be of $[900 - 1700]$nm.

We then define that the device should achieve a resolution of 3 nm, across the whole spectral range. This is extremely important in the d-scan application.

Furthermore, the device should be compact enough to be integrated in a d-scan commercial product. We thus set the maximum size of the spectrometer to 85.0 mm $\times$ 125.0 mm $\times$ 50.0 mm.

Besides that, the device should support a SMA optical fiber to be used as its input.

The production cost should also be kept under a budget of 3500 €.

Finally, it desirable that the device feature a self-managed library to interface with a *Windows* computer and that it supports the use of an external TTL trigger.

#	Requirement	Description	Priority
1	Spectral Range	Support a wavelength range of $[900 - 1700]$ nm.	Mandatory
2	Resolution	Achieve a resolution of 3 nm.	Mandatory
3	Size	Achieve dimensions no more than 85.0 mm $\times$ 125.0 mm $\times$ 50.0 mm.	Mandatory
4	Optical Fiber Connector	Support SMA optical fiber input.	Mandatory
5	Cost	Keep the total cost of the device under a budget of 3500 €.	Mandatory
6	Software	Self managed library to interface with a *Windows* computer.	Desired
7	External Trigger	Support external TTL trigger.	Desired

TABLE 5.1: Technical requirements for the development of an InGaAs spectrometer.

5.3 Design

5.3.1 Optical Design

The first step in the design phase of the InGaAs spectrometer is the definition of the optical configuration of the device. This definition is based on a custom take of the Czerny-Turner geometry. Instead of using two spherical mirrors, we make use of a parabola to fold the beam 90° from the entrance slit to the diffraction grating, as can be seen in Fig. 5.1. By using this approach, we are able to reduce the overall footprint of the device.

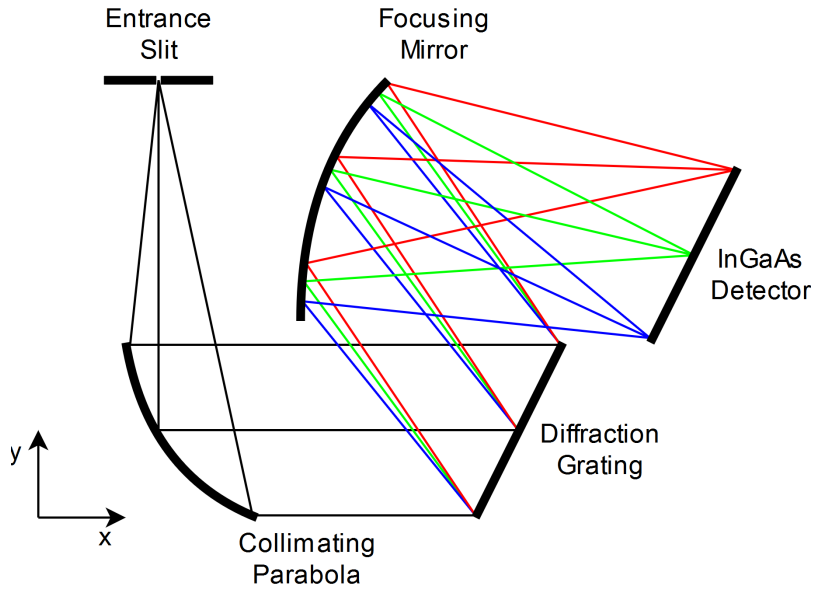

FIGURE 5.1: InGaAs spectrometer geometry. The footprint of the device is reduced by using a collimating parabola instead of a more typical spherical mirror.

In order to define the various distances and angles between the optical elements, ray-tracing simulations were developed using the Optometrika Matlab package [63]. These simulations aim to achieve a spectrometer design with the required wavelength range and resolution.

Taking into account the described geometry, we can make some considerations which will reduce the complexity of the simulations without impacting the final result. Firstly, by observing Fig. 5.1 one can see that, if the slit and parabola are well aligned (see Sec. 5.6 for details on what this means), the rays exiting the parabola are collimated. This means that we can place the source rays of our simulation on the parabola position without loss of generality. Secondly, since these rays are collimated, we see that the distance from the parabola to the diffraction grating is not critical to the operation of the device and should thus be left as a free parameter.

We are then left with five simulation variables: the angle of the diffraction grating, the angle and position of the focusing mirror and the angle and position of the detector. However, since these variables are all closely coupled, a simulation which computes all of them simultaneously would be too troublesome to implement. Furthermore, we can use a mere approximation of the parameters during the design process, since they can be further adjusted during the assembly process of the device. Thus, the variables were estimated using a combination of computational calculations and manual adjustments, for simplicity.

The following will go into detail on how the several possible adjustments of the simulation parameters impact the final result of the device.

5.3.1.1 Diffraction Grating Angle

Firstly, the angle of the diffraction grating can be shown to have a great impact on the spectral range of the spectrometer. A rotation of this angle effectively changes the incident angle θ_i in Eq. 2.10 and thus impacts the output reflected angle, θ_m, of each wavelength, λ. If the position and angle of the focusing mirror are both fixed, the range of wavelengths that hit the mirror surface is thus changed by a rotation of the diffraction grating angle, subsequently altering the spectral range of the light hitting the detector.

5.3.1.2 Focusing Mirror Position

The position of the optical elements on the bench will be explained using the coordinate system in Fig. 5.1. It can easily be seen that moving the focusing mirror in any direction has several consequences. Firstly, if moved in any direction, the spectral range of the obtained spectrum is changed, if we use the same reasoning as with the rotation of the diffraction grating. Secondly, moving the mirror along x direction impacts the critical focusing distance between the mirror and the detector, which needs to be taken into account when placing both of these elements. Finally, the mirror - and mirror mount - must not physically cover the beams travelling from the entrance slit to the parabola and from the parabola to the diffraction grating.

5.3.1.3 Focusing Mirror Angle

The focusing mirror angle is, as mentioned, closely coupled with both the angle of the diffraction grating and the angle of the detector. A change in the angle of the focusing mirror implies a change in the wavelength range that hits the detector. Because of this, that change must be compensated by a change in the angle of the diffraction grating, in order to guarantee that the spectral range of the device remains unaffected. These changes are also important in guaranteeing that the resolution of the spectrometer is nearly constant along the whole spectrum. Thus, for a single detector angle there is a unique combination of focusing mirror and diffraction grating angles which achieves the best resolution across the entirety of the desired spectral range.

Furthermore, this angle is also important in compactly placing the detector mount, behind the diffraction grating, ultimately reducing the footprint of the device.

5.3.1.4 Detector Position

The detector position should reflect the choices made for the other variables presented above. Firstly, the detector must be placed away from the focusing mirror at a distance that is approximately the focusing distance of this element. However, the focus of the spherical mirror is astigmatic, due to the nature of the spectrometer geometry, which can be used to our advantage in improving the resolution of the device, if the distance between the two elements is chosen such that the beam spot is as shown in Fig. 5.2 a).

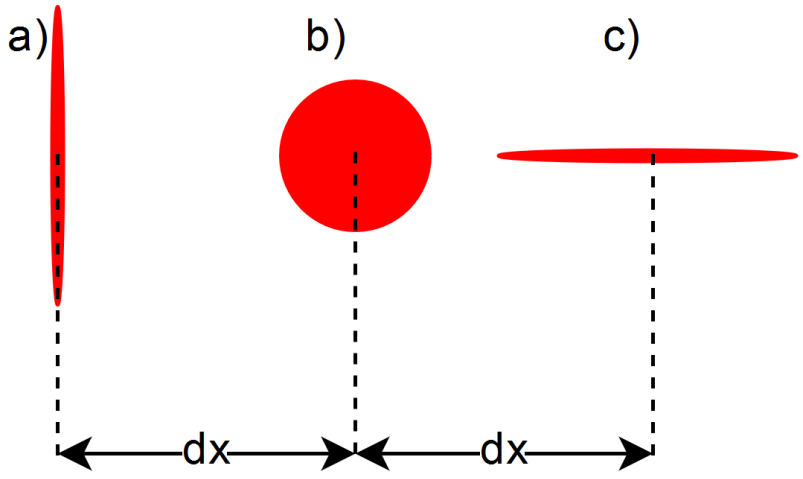

FIGURE 5.2: Astigmatic focus on the detector. By increasing the distance between the mirror and the detector, the beam spot on the array goes from *a)* to *b)* to *c)* where the *b)* position is for the exact focusing distance of the mirror. Beam spot sizes are not to scale.

5.3.1.5 Detector Angle

Finally, the detector angle helps reducing the path difference for rays incident on opposing sides of the focusing mirror, thus allowing all rays from any specific wavelength to be focused on the same spot on the detector.

5.3.1.6 Optical Design Results

After taking into consideration all of the determinant factors explained above, we arrived at the following results from the ray-tracing simulations. In Fig. 5.3 we can see the path of the design central wavelength, 1300 nm, through the various optical elements. Notice that the source rays are originating from the parabola position and they are assumed to be collimated by that element, thus neither this element nor the entrance slit are present on the simulation. An important take from Fig.5.3 is that the rays are focused on approximately the center of the detector, as desired since their wavelength should mark the center of the spectral range.

We then moved on to performing a simulated scan of the spectral range in order to estimate the resolution of the device. Fig. 5.4 shows the result of such scan. We can imediately notice that the peaks are well defined across the whole spectrum, having a FWHM of approximately 3 to 4 pixels. However, we can also discern that the peaks of a smaller wavelength (900 nm and 1100 nm) are slightly less resolved than the other two. Even though the overall resolution of the peaks could be improved by further actuating of the simulation variables, these parameters can be later optimized in the calibration of the final device and are thus left unchanged at this stage.

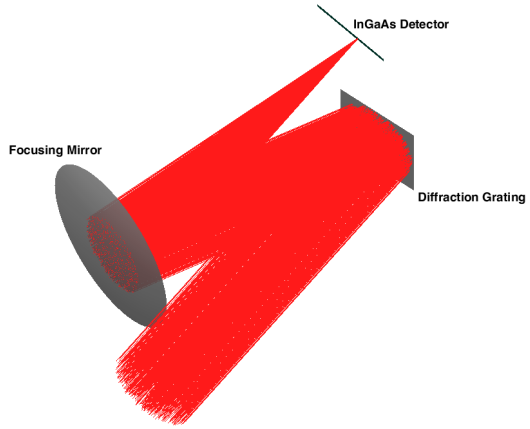

FIGURE 5.3: Ray tracing of the central wavelength of the spectrometer, 1300nm.

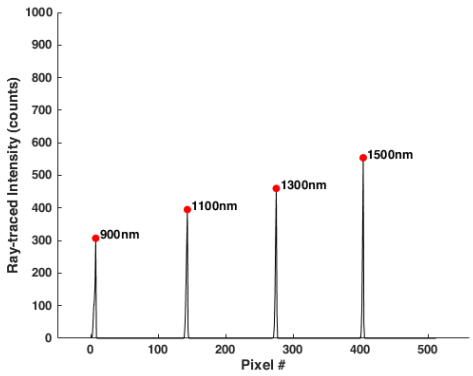

FIGURE 5.4: Resolution prediction of peaks across the simulated spectral range of the designed spectrometer.

5.3.2 CNC Part Design

The next step in the design process of the spectrometer was the 3D drawing of the custom parts required for the prototype. A computer numerical control (CNC) machine allows us to manufacture custom designed parts. By manufacturing the optical component mounts using the CNC technique, we can design parts with a small footprint.

Additionally, we can design the mounts according to the required adjustment points for each optical component, thus facilitating the assembly and tuning of the device (see Sec. 5.9).

A custom enclosure was also designed to ensure the robustness of the device. In order to accurately place the optical component mounts, several grooves were machined on the base of the enclosure. These placement references are of extreme importance during the assembly of the prototype (see Sec. 5.6).

The 3D part design results can be seen in Fig. 5.5. We can see that the final design of the device features an external size of 120.0 mm $\times$ 75.0 mm $\times$ 47.0 mm, if we disregard the protruding of the PCB, which can be replaced in a future version of this spectrometer.

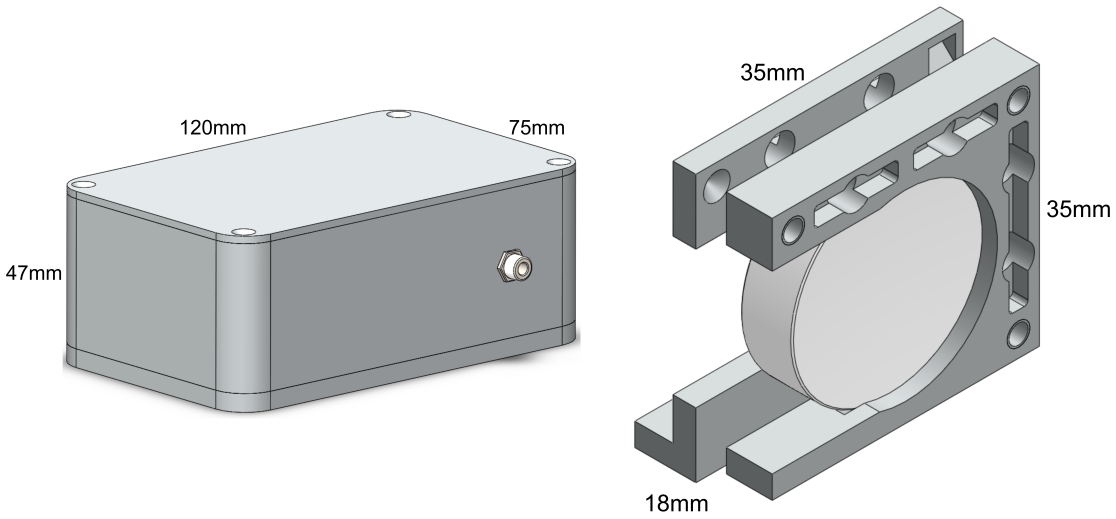

FIGURE 5.5: Result of the 3D drawings of the prototype spectrometer.

The custom mirror mount for the 1" focusing mirror is also presented in Fig. 5.5. The mount is composed of two parts (front and back) which are connected through the use of springs attached to small metal pins, inserted on the designed slots (seen on the front piece, in the figure). By doing this, the assembly supports several degrees of freedom on the movement of the component due to the three adjustment screw positions, on the corners of the mount. This use of separate parts, with springs and screws as connectors,

is common among commercial mirror mounts, however, none of the considered ones are as compact as this one, with dimensions of 35.0 mm × 18.0 mm × 35.0 mm (for 1" optics). This compact design enables the reduced size of the developed spectrometer.

5.4 Table-top Demonstrator

5.4.1 Assembly

The next step in the development process it to verify the ray-tracing simulations and make sure that the device is feasible, using a table-top demonstrator. However, this assembly is still far from the final device since it uses commercially available mounts to place the optical elements, instead of custom designed ones. Due to this reason, the demonstrator was larger in size and much harder to implement than the final prototype due to physical restrictions originating from the commercial mounts.

The optical components used in this assembly are the following:

- Entrance slit: 1", $W_s = 50\,\mu m$
- Parabola: 1"
- Diffraction grating: 25 mm × 25 mm
- Focusing mirror: 1" spherical silver mirror
- InGaAs detector: $N_p = 512$ pixels, $W_p = 25\,\mu m$

In order to assemble the demonstrator, a reference alignment beam from a helium neon (HeNe) continuous wave (CW) laser was used. The process begins with the alignment of the entrance slit and the collimating parabola. We then moved on to placing the diffraction grating on the center of the beam coming from the parabola at a convenient position, since this is not a critical distance to the alignment of the device. Afterwards, we roughly positioned the focusing mirror so that the second order reflection from the grating ($2\lambda = 1265.6$ nm, close to the 1300 nm design central wavelength) was centered on the mirror. Finally, the detector was placed close to the focusing distance of the mirror and at, approximately, the simulated angle. The alignment process of the device will be further detailed in Sec. 5.6.

5.4.2 Table-top Demonstrator Results

At this point, we switched the light source to a mercury pen lamp [64] in order to observe the emission spectrum on the spectrometer. After careful tuning of the diffraction grating, focusing mirror and detector, we arrived at the spectrum in Fig. 5.6. We can easily notice that the resolution of the device is far from being ideal since the spectral lines have a FWHM of approximately 20 nm, far from the 3 nm proposed as the requirement of the device. However, this can be justified by the physical constraints existent in the table-top assembly itself. Since the distances between the optical elements are relatively small, they are impossible to be attained with the commercially available posts and mounts used in this demonstrator. Furthermore, we had no method of precisely measuring the distances and angles between the optical elements in order to place them in the simulated positions. Because of this, we accepted the result in Fig. 5.6 as a mere indication that the concept of the device is achievable, using the same geometry as in the ray-tracing simulations. We can thus assume that the results from the simulations will transfer to the final product, using the custom designed mounts and enclosure which allow us to precisely place the optical components.

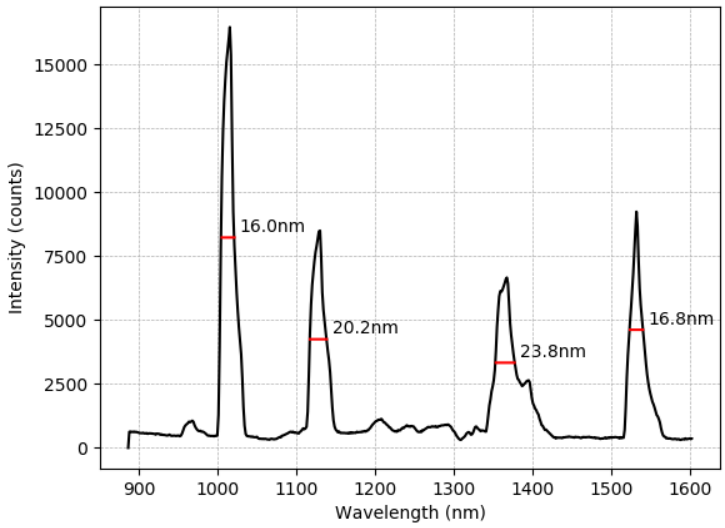

FIGURE 5.6: Hg lamp hot spectrum acquired with the table top demonstrator.

5.5 Optical Component Choice

In order to fulfil the requirements set for the spectrometer under development, several changes had to be made regarding the optical components used in the table-top demonstrator, when the development moved to the prototype phase.

Firstly, the entrance slit used in the demonstrator is not adequate to allow for a 3 nm resolution. According to Eq. 2.11, a 50 µm entrance slit achieves a resolution of 9.4 nm, using the same detector - 512 pixels, 25 µm pixel width - and the same wavelength range - $[900 - 1700]$nm. Therefore, the entrance slit used in the prototype should have a width of 15 µm, which allows for a resolution of 2.8 nm.

Furthermore, the parabola was changed to a $1/2$" diameter one and the diffraction grating changed to a $1/2" \times 1/2"$ one, in order to achieve the most compact design as possible.

The final list of components for the prototype spectrometer is, thus, as follows:

- Entrance slit: 1", $W_s = 15\,\mu$m
- Parabola: $1/2"$
- Diffraction grating: $1/2" \times 1/2"$
- Focusing mirror: 1" spherical silver mirror
- InGaAs detector: $N_p = 512$ pixels, $W_p = 25\,\mu$m

5.6 Prototype Assembly

Having selected the components and manufactured the custom mounts, we may begin with the assembly process of the prototype. This process began in the same way as with the table-top demonstrator: with the alignment of the parabola. The first step is thus to attach the parabola to the custom design mount and securing the assembly to the base of the spectrometer, making sure to use the reference grooves.

In order to facilitate this alignment and to serve as a reference for the rest of the assembly, a HeNe laser was used. Two guiding mirrors were used to make the beam parallel to a line following the holes on the surface of the optical table and to center the beam on the parabola. This process allows us to align the parabola so that the reflected beam is both perpendicular to the reference one and parallel to the table. It is important to note that

each time the parabola is moved, one should recenter the reference beam on the parabola while keeping it parallel to the optical table. If this step is disregarded, one could be misaligning the parabola and causing unwanted aberrations on the final product, due to the parabola being aligned for an off-center beam and not the centered one coming from the entrance slit.

The next step in the process is the alignment of the entrance slit with the parabola. In this step we must consider that the entrance slit should be aligned with the center of the parabola while at the same time being aligned with the center of the fiber coupling hole on the outside walls. With these two goals in mind, we designed a 3D printed part to place the slit exactly aligned with the fiber input.

In order to align the slit, the device was placed close to the second guiding mirror for the reference beam. By inciding this beam on either the parabola or the entrance slit, one can observe the diffraction pattern and use it to align the slit and parabola assembly. If the centers of the two elements are not both coincident with the beam, the diffraction pattern will appear focused on one side and blurry on the other. This is better observed by inciding the reference beam on the parabola and observing the image of the slit far away from the assembly (see Fig. 5.7 a)). Furthermore, if the slit is tilted to either side, both the individual lines and the whole pattern will reflect that and have the same tilt. To observe this, the entrance slit can be imaged on a surface close to the assembly by, again, inciding the reference beam on the parabola (see Fig. 5.7 b)). Finally, one can rotate the device by 90° in order to incide the reference beam on the entrance slit and observe the diffraction pattern of the slit after the light is collimated by the parabola. This setup allows us to finely adjust the tilt of the entrance slit by making the diffraction pattern lines parallel and vertical. It also allows for the adjustment of the center alignment of the two elements since the pattern lines will appear to curve, and not be completely vertical, if there is any misalignment in this parameter (see Fig. 5.7 c)).

The following step in the assembly requires the placement of the grating. After gluing the grating to the custom designed mount, we placed the optical component on the base of the device and identified the diffraction orders by observing the relative intensity of the reflected pattern - the 1^{st} and 2^{nd} orders of the grating are the higher in intensity.

The focusing mirror was then glued to its respective mount and placed on the assembly, once again using the reference grooves on the base of the assembly. Here, we made sure that the adjustment screws were all in the zero position since this will help in the

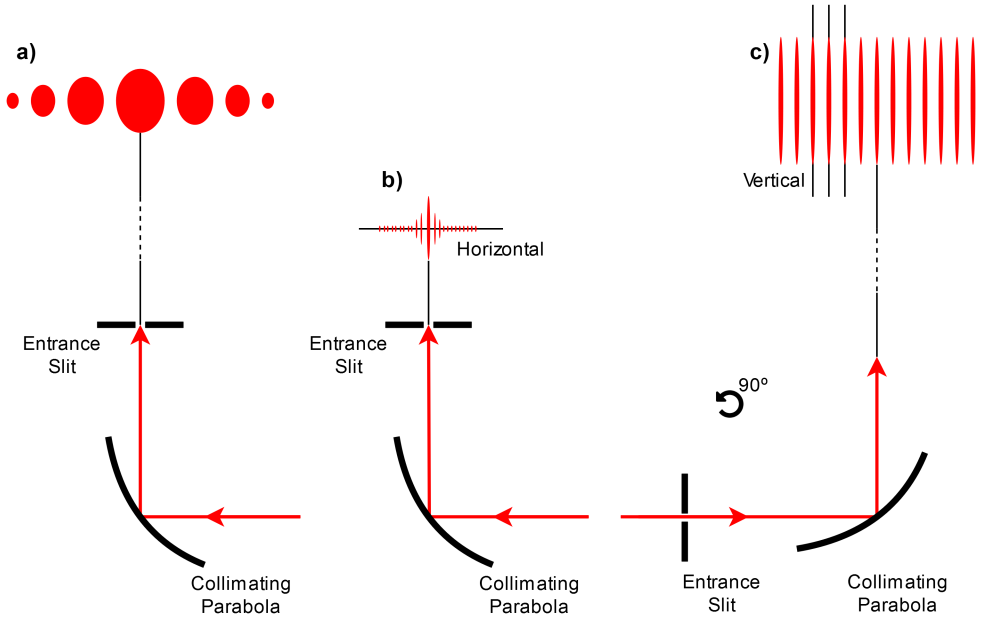

FIGURE 5.7: Slit and parabola alignment diffraction pattern. a) Reference beam incident on parabola and image of the entrance slit observed far away from the setup. b) Image of the slit if observed close to the setup. c) Reference beam incident on the entrance slit and diffraction pattern observed far away from the setup.

alignment of the mirror, by exactly knowing the direction in which we should rotate the screws. We then repeat the procedure used for the table-top demonstrator and estimate the position of the diffraction grating by centering its 2^{nd} order reflection on the focusing mirror.

Finally, the InGaAs sensor was placed on the control PCB and mounted on the assembly. The detector mount has no adjustment screws and is thus fixed to the position resulting from the ray-tracing simulations.

5.7 Control Software

In order to control the spectrometer via a computer and thus be able to integrate it in the d-scan software, a *C++* library was developed to implement the required features. This library implements the following functions:

```
DWORD GetNumDevices(DWORD *dwNumDevices);
```

Retrieves the number of spectrometer devices connected to the computer. This numbering is used to select the device which we want to control.

`DWORD OpenDevice(DWORD dwDeviceNum, DWORD_PTR* dwDeviceHandler);`

Opens a connection with the device selected by *dwDeviceNum* and associates a device handler with that device. The handler will be used by all the other functions, to control the device.

`DWORD GetNumPixels(DWORD_PTR* dwDeviceHandler, DWORD* dwPixelNum);`

Returns the number of pixels on the detector of the device. This parameter is important in defining the size of the arrays to save the acquired spectra.

`DWORD SetIntegrationTime(DWORD_PTR* dwDeviceHandler, float fIntTime);`

Sets the integration time of the device, returning an error if the value provided is out of bounds.

`DWORD SetNumAverages(DWORD_PTR* dwDeviceHandler, DWORD dwNumAver);`

Sets the number of averages to be performed for the acquisition of each spectra.

`DWORD GetDark(DWORD_PTR* dwDeviceHandler, INT32* DarkArray);`

Waits for the user to cover the entrance of the spectrometer in order to acquire a *dark* spectrum. This data can then be subtracted to the acquired spectra to perform a *dark* calibration of the device.

`DWORD GetSpectrum(DWORD_PTR* dwDeviceHandler, INT32* SpectrumArray);`

Acquires a spectrum, with the set integration time and number of averages. Saves the spectrum to the *SpectrumArray* variable.

`DWORD CloseDevice(DWORD_PTR* dwDeviceHandler);`

Closes the connection to the device with handler *dwDeviceHandler*.

These functions provide a basic pipeline for the acquisition of spectra using the custom device. However, more functions are implemented in the library to, for example, save the spectra to a file and *get* functions for the integration time and number of averages.

In the future, the library should be able to manage the connection to the device by using its serial number as a reference. This way, the library could, for example, re-connect to the device if the *USB* connection is lost for a brief moment.

Furthermore, to help in the tuning process, I developed a *Python* software which takes the acquired spectra and displays them on the computer screen. This software computes and displays the FWHMs of the peaks in the spectra, thus allowing the user to have feedback on the impact of the adjustments on the resolution of the device.

5.8 Experimental Setup

In order to calibrate the device and accurately assess its performance, a rigorous experimental setup had to be used. This setup consists of a light source coupled to a NIR designed optical fiber - 200/230 µm, IR-VIS, multimode - which then attaches to the SMA connector on the spectrometer (see Fig. 5.8). In this setup, five light sources were used: a diode-pumped solid-state (DPSS) CW laser, a mercury vapor UV lamp, a tunable CW laser, a white light lamp and a fluorescent lamp.

The DPSS laser was used due to its well defined wavelength ($\lambda = 1064\,\text{nm}$) and high intensity. This laser will serve as a reference for the wavelength to pixel number matching and as a measure for evaluating the resolution during the tuning of the device.

Furthermore, the mercury UV lamp provides several lines in the design wavelength range of $[900 - 1700]$nm and is thus used to assess the resolution of the device across the whole spectral range. This light source, together with a fluorescent lamp, will also be used to establish a comparison between the device under development and a commercially available spectrometer of the same characteristics.

Finally, the white light source will be used to perform an intensity calibration of the device.

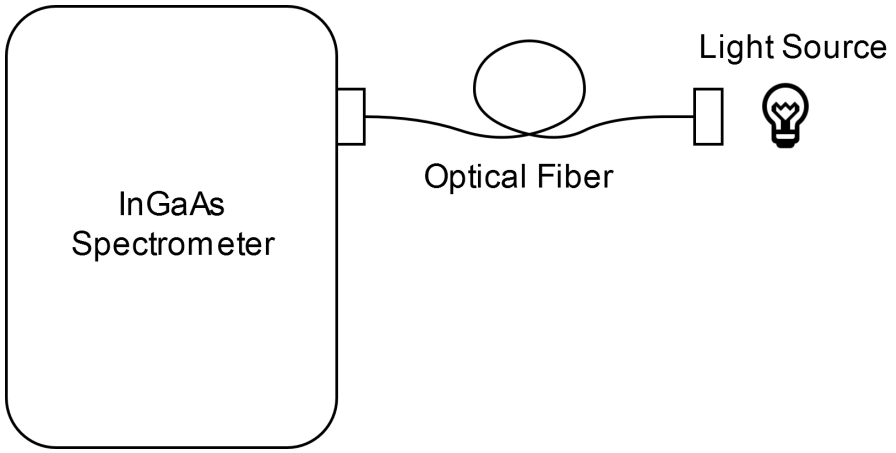

FIGURE 5.8: Experimental setup used to tune, calibrate and assess the performance of the InGaAs spectrometer.

5.9 Prototype Tuning

The tuning of the device is the most defining step in the assembly since it will ultimately determine its performance. The main goal of this step is to find the positions for the grating and focusing mirror to achieve the spectral range and resolution requirements for the device.

It is important to note that, while performing this tuning, we could be forced to make adjustments to the parabola tilt and to the position of the slit since they can be much finely adjusted at this point, once all the other optical elements are in place.

During the tuning process, the *Python* software will be used as a means of obtaining feedback on the adjustments made by looking at the spectrum of the light source and the resolution of peaks.

The first step towards the tuning of the device is to maximize the signal of the DPSS laser. Note that, when working with any laser light source, we should make sure that the integration time of the detector is set to its minimum - 100 µs - in order to protect the sensor from the high intensity of the laser beam.

At this point, we want to estimate the pixel on which the light from the DPSS laser would incide, if the device was tuned to the desired wavelength range, $[\lambda_i, \lambda_f]$. Assuming that the wavelength to pixel number calibration is approximately linear, we can use Eq. 5.1 with $\lambda_{DPSS} = 1064\text{nm}$, $\lambda_i = 900\text{nm}$, $\lambda_f = 1700\text{nm}$ and $Number\ of\ Pixels = 512$ to conclude that $Pixel\ \#_{DPSS} \sim 100$. Using this result, we can then rotate the grating so that the signal from the laser is around pixel number 100.

$$\frac{\lambda_{DPSS} - \lambda_i}{\lambda_f - \lambda_i} \sim \frac{Pixel\ \#_{DPSS}}{Number\ of\ Pixels} \tag{5.1}$$

We can proceed by finding the position of the focusing mirror which focuses the DPSS laser light on the detector. To achieve that, we start rotating the screws on the mirror mount while trying to improve resolution and maximize the signal strength. During this process, it is important to tighten the screws in the same direction and by approximately the same amount since we want to actuate only on the distance between the focusing mirror and the detector and not on the angles involved. Once the resolution of the signal is close to the required value of 3 nm, we can move on to the next step.

The following step in the tuning process consists of observing the emission pattern of the mercury UV lamp in order to assess the resolution of the spectrometer across its

spectral range. Here, we increased the integration time of the detector to $\sim 100 - 200$ms to compensate the reduced intensity of this light source when compared to the DPSS laser.

Using this light source, we can define the angle between the grating and focusing mirror which improves the overall resolution. It should be noted that, after the previous step, the widths of the mercury lamp lines around the DPSS laser wavelength should be close to optimal, while the resolution of the device on the longer wavelengths is, most likely, far from ideal. To achieve a balance for the resolution across all wavelengths, we rotate the focusing mirror so that we defocus the shorter wavelengths and focus the longer ones. Note that, as established in the design phase of the device, the rotation of the focusing mirror should be compensated by an opposite one of the diffraction grating, in order to preserve the desired spectral range.

At this point, we performed an iterative process, switching between the DPSS laser and the mercury vapor lamp. We aimed to improve the resolution of the mercury lamp lines by actuating on the distance between the mirror and the sensor while using the DPSS laser as a reference point for the wavelength range.

Here, we should reach a plateau where the overall resolution can't be further improved by actuating on the focusing mirror distance and angle and on the diffraction grating angle. Therefore, we have to consider adjusting the remaining parameters: the position of the entrance slit, the tilt of the parabola and the tilt of the diffraction grating. By moving the entrance slit, we should be able to better center it relative to the core of the optical fiber and the center of the parabola, which should greatly improve both the signal strength and the resolution of the device. Furthermore, by changing the tilt of both the parabola and the diffraction grating we can correct aberrations caused by the beam not being parallel to the base of the spectrometer.

After this last step and some more iterations of the focusing mirror angle and distance, we should arrive at the required resolution of 3 nm while having sufficient signal strength with the DPSS laser - $\sim 80\%$ of saturation - at an integration time of 100 µs.

5.10 Prototype Calibration

The calibration of the device is the last step in the production process. The developed prototype was calibrated in terms of wavelength and intensity.

5.10.1 Wavelength Calibration

In order to correctly measure the spectrum of a light source, a correspondence has to be made between the pixels on the detector and the wavelengths of the light. To do so, we must take light sources with well defined peaks at certain wavelengths across the spectral range of the spectrometer and observe the detector pixel number at which said peaks occur. The peaks used for the calibration of this device are documented in Fig. 5.9. This calibration uses light from three different sources: a mercury vapor lamp, a DPSS CW laser and a tunable CW laser. In the case of the mercury vapor lamp, the peaks wavelengths were measured with a calibrated state of the art spectrometer, since we did not find any documentation for the emission spectrum of the lamp in the NIR region. Both the DPSS and tunable lasers used were assumed to be correctly calibrated to their respective wavelengths.

After acquiring spectra from the three different sources, we can match the known wavelengths of the peaks to the pixel number at which they occur. A second-order polynomial fit was then performed on the data, establishing a model to predict the wavelength corresponding to any pixel on the detector - higher order contributions are usually negligible. The result of polynomial fit is shown in Fig. 5.10. As expected, the fit function is mostly linear, having a second-order parameter $\sim 10^4$ times smaller than the first-order one. Finally, by computing the $R^2 = 0.99998$ we can confirm that the second-order polynomial model correctly predicts the wavelength to pixel number relation.

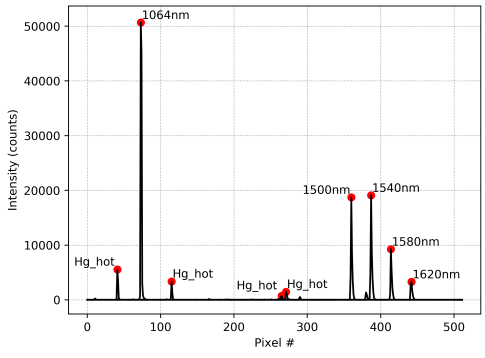

FIGURE 5.9: Source peaks used for the wavelength calibration of the developed spectrometer. Here, it was important to choose sources with well defined peaks across the whole spectral range.

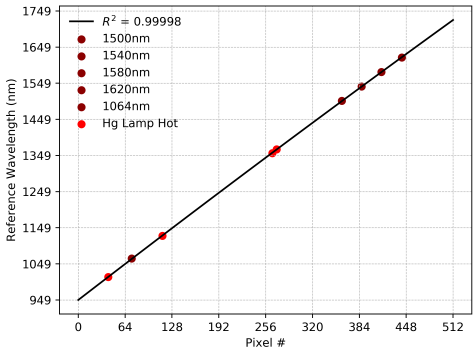

FIGURE 5.10: Second-order fit of pixel number to wavelength which provides the wavelength calibration for all the pixels on the array. We can see that the fit is mostly linear, as expected.

The wavelength calibration also allows us to predict the spectral range of the device. In the case of this prototype, this is $[950.5 - 1722.5]$nm, achieving the desired range within a tolerable margin.

5.10.2 Intensity Calibration

The next step in the calibration of the device is to calibrate the relative intensity of the light incident on different pixels on the detector. Due to the geometry of the spectrometer, not all pixels receive the same amount of light, even if the light source is uniform across the wavelength range. Thus, this intensity calibration is an important step in correcting such an intrinsic characteristic and in obtaining reliable data from the spectrometer.

The calibration procedure begins with acquiring the spectrum of a white light lamp. Then, the theoretical spectrum of a black body at the temperature of the lamp - in this case $2900K$ - is computed across the spectral range of the device. By taking the acquired spectrum and dividing it by the theoretical one, we obtain a calibration factor for the intensity of each pixel (Fig. 5.11). It is important to note that this factor is highly dependent on the wavelength corresponding to each pixel and should thus be recalculated whenever the wavelength calibration is changed.

Finally, in order to be able to establish a comparison between a state of the art spectrometer and our prototype, the same intensity calibration procedure should be done with the commercial spectrometer, using the same optical fiber and white light source (Fig. 5.12).

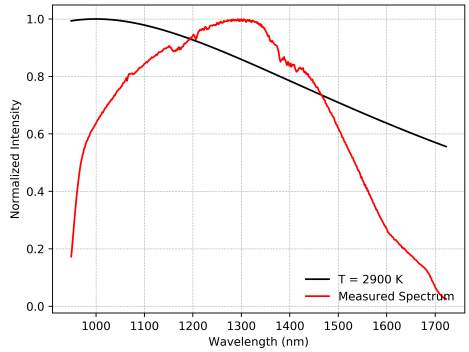

FIGURE 5.11: Intensity calibration of the developed spectrometer.

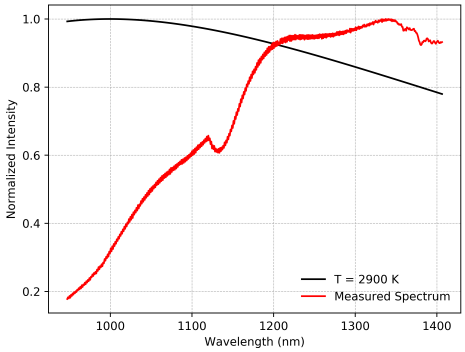

FIGURE 5.12: Intensity calibration of the state of the art spectrometer.

5.11 Results

In this section, we will present the final results of acquiring spectra with the developed prototype spectrometer. We will also present a comparison between our prototype and a state of the art spectrometer, as previously mentioned. Lastly, we will comment on the fulfilment of the requirements set for the device.

5.11.1 Resolution

In order to correctly assess the resolution of the device we have to use a light source with spectrum peaks across the entirety of the wavelength range. These peaks must also have a smaller linewidth than the resolution of the spectrometer, as previously stated. For that, the mercury vapor lamp was once again used since it fits both criteria [64]. In Fig. 5.13 we can see that the peaks of the emission spectrum of the lamp have a width close to the required 3 nm. Here, the resolution of the peaks is calculated using Eq. 5.2, where λ_i and λ_f are, respectively, the starting and ending wavelengths of the spectrometer's range, according to the wavelength calibration.

$$Peak\ Resolution = \frac{FWHM}{Number\ of\ Pixels\ on\ the\ Detector} \times (\lambda_f - \lambda_i) \tag{5.2}$$

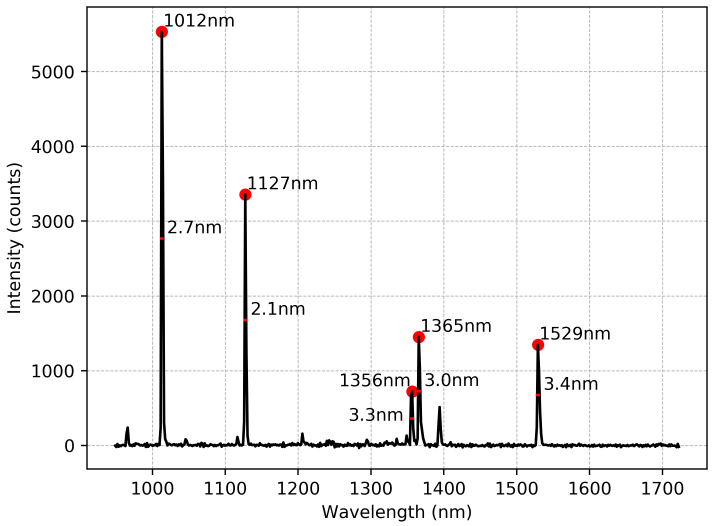

FIGURE 5.13: Developed spectrometer resolution of the mercury vapor lamp emission lines.

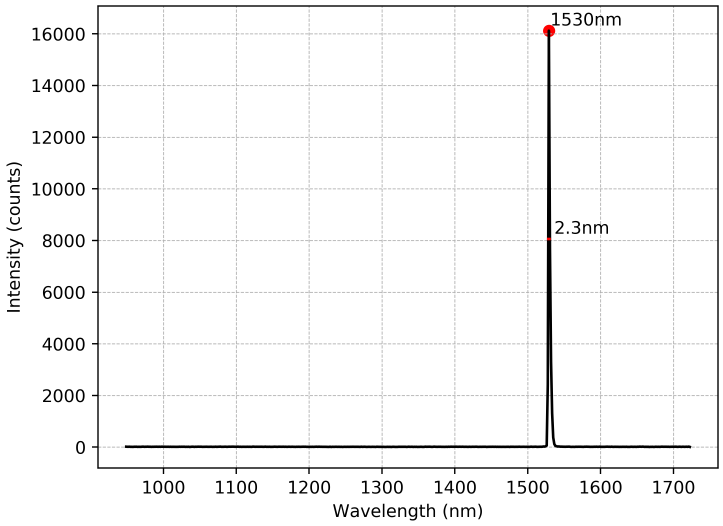

FIGURE 5.14: Developed spectrometer resolution of the tunable laser at 1530 nm.

We can see that, in the mercury lamp spectrum, the peaks of lower wavelength (e.g. 1012 nm and 1127 nm) seem to be better resolved than the peaks of higher wavelength (e.g. 1529 nm). However, in Fig. 5.14 we can observe that, for a laser spectrum at 1530 nm, the spectrometer has a resolution of 2.3 nm. This can be readily explained by taking into account the binning effect of having a discrete number of pixels on the InGaAs sensor. Since the spectrum of a given light source is continuous in wavelengths, we can easily see that there is a possibility that some wavelengths hit the detector between two pixels of the array. When this happens, such a wavelength is, intrinsically, less resolved. This effect can be better understood by observing Fig. 5.15 where the tunable laser was used to scan the short wavelength range of $[1590.0 - 1591.2]$nm and where we can clearly see the effect of binning on the resolution of the peak.

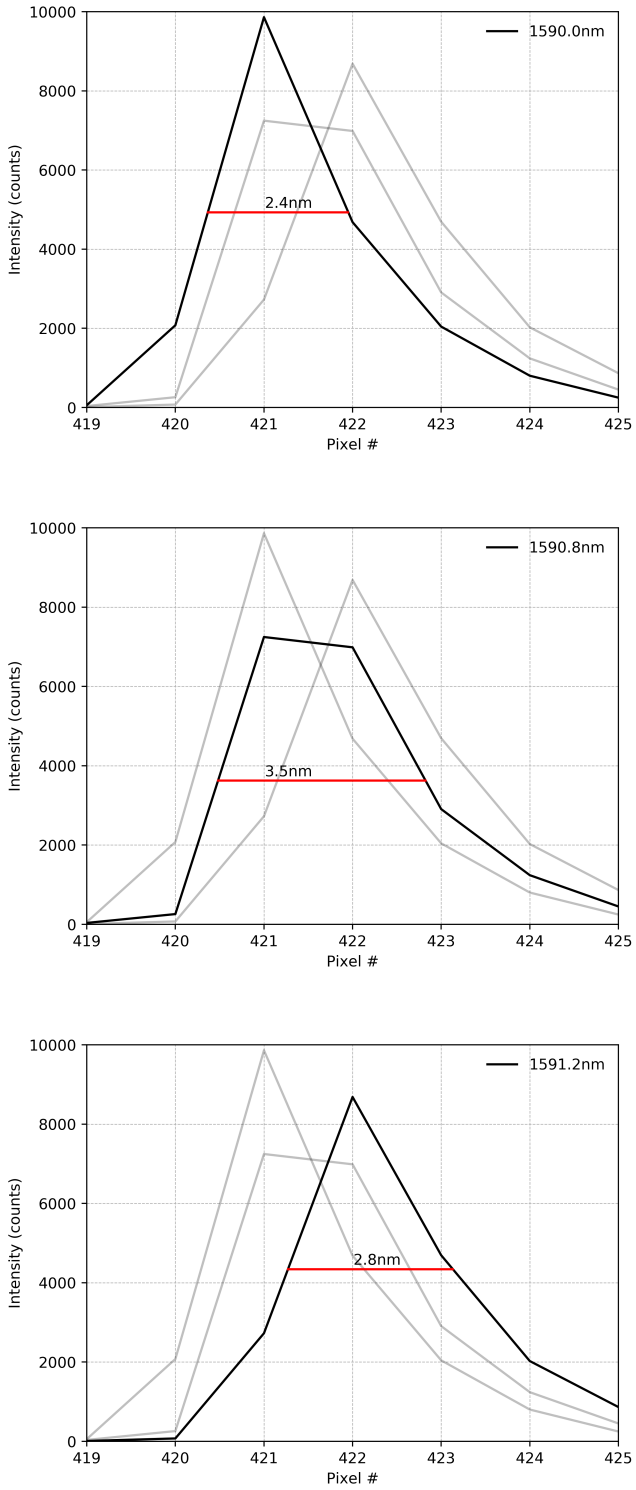

FIGURE 5.15: Effect of pixel binning on the resolution of the tunable laser at [1590.0 – 1591.2]nm. If a certain wavelength is incident in the middle of two pixels, they will both capture some amount of light and thus the device is not able to properly resolve the line.

5.11.2 State of the Art Comparison

The final result taken from the analysis of the prototype is a comparison with a state of the art spectrometer of the same characteristics. To do so, the spectrum of both the mercury vapor lamp and the fluorescent lamp were taken with both spectrometers.

We begin by computing the resolution of the emission lines of the mercury vapor lamp, acquired with the reference spectrometer. We can see that the resolution is below the reference 3 nm threshold, as expected (Fig. 5.16). However, this spectrometer has a much smaller spectral range ($\sim [900 - 1400]$nm) than the prototype developed in this work ($\sim [900 - 1700]$nm) which factors into the higher resolution of the device, according to Eq. 2.11.

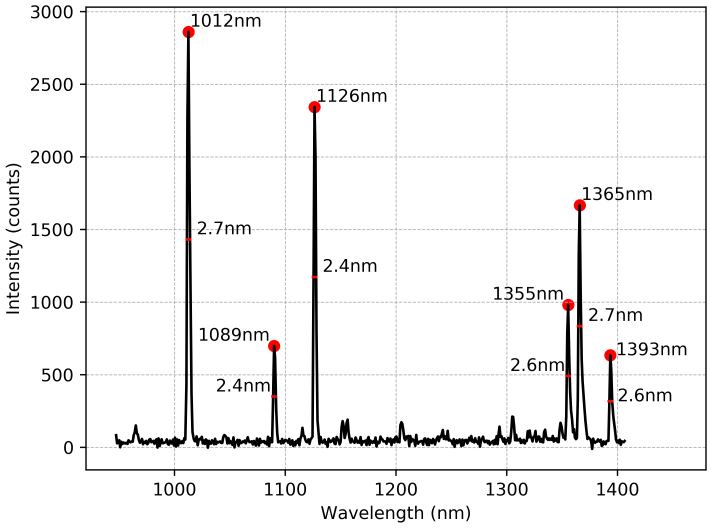

FIGURE 5.16: State of the art spectrometer resolution of the mercury vapor lamp emission lines.

We then overlapped the spectra obtained with the two different spectrometers, from each light source. To have a sense of the deviation of the prototype from the reference spectrometer, we applied both the intensity and wavelength calibration to the data. The results are shown in Fig. 5.17. From the two overlapped spectra, we can qualitatively see that the spectrometers return approximately the same spectrum, in terms of wavelength and, in the case of the mercury lamp, also in intensity of the spectrum. However, we can also immediately see that in the spectrum of the mercury vapor lamp of the reference spectrometer, an extra peak appears at around 1100 nm, which does not appear in the developed prototype spectrum. We initially thought that the detector could have some

malfunctioning pixels around that region, however, that would have been made apparent when the white light spectrum was measured for the intensity calibration. The reason of the discrepancy is still yet to be unfolded and further testing is required to determine its origin.

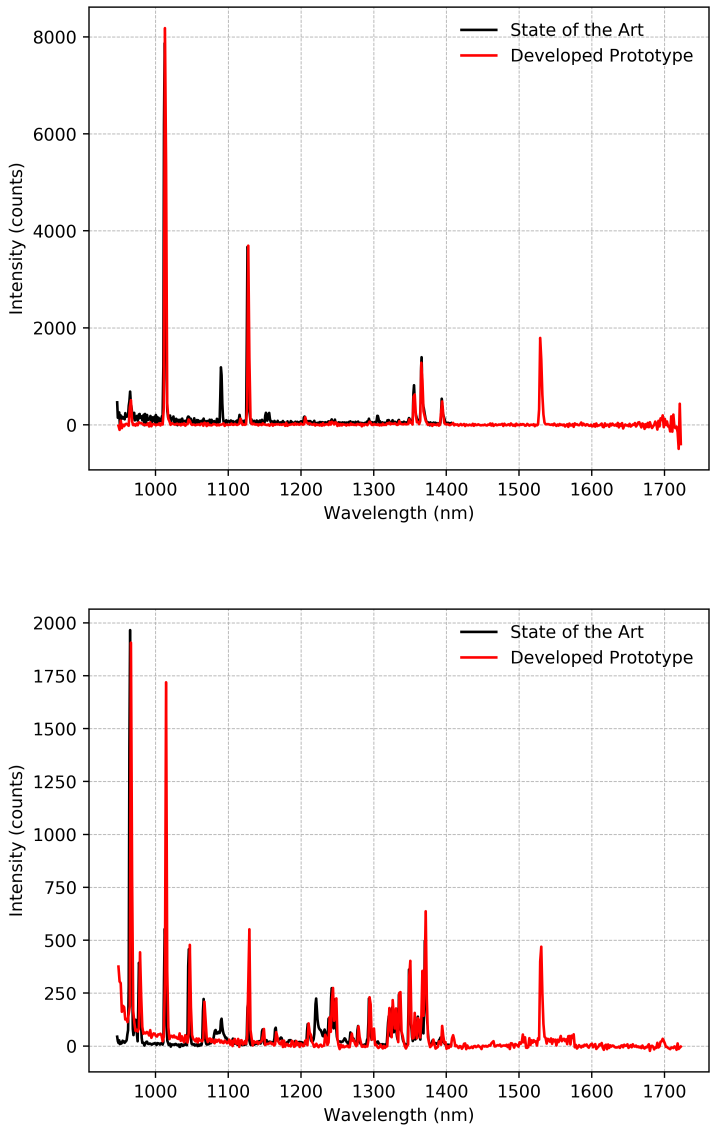

FIGURE 5.17: Comparison between the developed prototype and the state of the art spectrometer. Top: mercury vapor lamp spectrum. Bottom: fluorescent lamp spectrum.

From the fluorescent lamp data, we can see that the two acquire spectra agree in terms of wavelength and intensity, in the majority of the spectral range. However, the peak of wavelength a little over 1000 nm shows a local inconsistency in terms of intensity. Furthermore, we can again notice the missing peak close to the 1100 nm and a new one above

the 1200 nm. Future work must be done to understand the origin and correct these two discrepancies.

5.11.3 Requirements Fulfilment

The final step in the verification of the developed prototype is to evaluate the fulfilment of the initial requirements, following Table 5.1.

We begin by analysing the spectral range of the device. As mentioned in Sec. 5.10.1, the achieved wavelength range of the spectrometer is $[950.5 - 1722.5]$nm. This is a range of 772 nm, which is only 3.5 % less than the established 800 nm. This is an acceptable error since this range could be further adjusted in a future version of the spectrometer and thus we can say that this requirement has been fulfilled. The achieved spectral range is also higher than the one in the state of the art spectrometer used for comparison purposes.

Moreover, the required resolution of $\sim$3 nm was achieved, as can be seen in Sec. 5.11.1. Additionally, this resolution was obtained with a high spectral range and across the entire spectrum of a source.

Furthermore, the prototype has a footprint of 75 mm $\times$ 120 mm, which fulfils the set requirement for the footprint of the device. However, the control PCB for the detector has a height of $\sim$50 mm which imposes a limit to the compactness of the device in volume. Future work should be done in developing a more compact version of this PCB.

An SMA optical fiber connector has been implemented in the developed prototype, as required.

The cost target of 3500 € was achieved for the current prototype. For a new version of the device with a different PCB, the cost will be re-evaluated, but we do not expect a significant change given the low cost of electronics compared to the remaining components. The price of the final device is one of the primary achievements of the development process since a state of the art device is more than twice as expensive, which has an impact in the overall cost of production of the d-scan product.

Besides that, a software library to manage the device is in the early stages of development. The library has already been used to perform the most basic of features of the spectrometer (e.g. setting integration times and acquiring spectra) but is not ideal in managing the serial connection to the spectrometer.

Finally, even though the detector PCB allows for external triggering, this feature has not been implemented in this version of the device and has thus been left for future development.

#	Requirement	Achieved	State of the Art
1	Spectral Range	Yes. $[950.5 - 1722.5]$nm.	$\sim [900 - 1400]$nm.
2	Resolution	Yes. $\sim$3 nm.	$\sim$3 nm.
3	Size	Yes. 75.0 mm $\times$ 120.0 mm.	70.5 mm $\times$ 104.0 mm.
4	Optical Fiber Connector	Yes.	Yes.
5	Cost	Yes. $<$3500 €.	More than 2x as much.
6	Software	Yes. Can control device but not manage the USB connection.	Yes.
7	External Trigger	Not implemented.	Yes.

TABLE 5.2: Fulfilment of the set requirements for the development of an InGaAs spectrometer.

5.12 Chapter Review

A high resolution InGaAs spectrometer was developed as part of this project.

We begin the chapter by setting the technical requirements of the device which will serve as figures of merit of the final prototype. The three most important requirements are the spectral range ($[900 - 1700]$nm), the resolution (3 nm) and the size (85.0 mm $\times$ 125.0 mm $\times$ 50.0 mm).

In the design phase of the device, we defined the optical geometry and performed ray-tracing simulations to set the positions of the optical elements. These simulations helped us conclude on the impact of each degree of freedom on the final spectrum acquired. Using the results of these simulations we designed custom mounts for the optical elements to facilitate the assembly of the device and to make it as compact as possible.

We then moved on to assembling a table-top demonstrator of the spectrometer, which proved useful in securing the feasibility of the device, using the geometry defined in the design phase. However, because of the physical restrictions involved when using commercially available optical mounts, we were not able to accurately verify the ray-tracing simulations, thus obtaining a not so ideal resolution of $\sim$20 nm.

Moreover, we present the *C++* software built to control the spectrometer. This library implements a full pipeline for the acquisition of spectra with the device. This library is also used together with a simple *Python* script to help in the tuning of the device by continuously acquiring spectra and measuring the resolution of the spectrometer.

In order to be able to achieve the desired resolution of 3 nm, we were required to make changes to the optical components used, when the project was transferred to the prototype phase. Because of this, a slit of 15 µm width was used in the final device. Additionally, the parabola and diffraction grating were changed to more compact versions.

Furthermore, we proceeded with the assembly of the prototype spectrometer. Here, a HeNe laser was used as a reference beam for the alignment of the parabola and entrance slit and for the rough positioning of the remaining optical elements.

Then, an experimental setup was defined as part of the prototype tuning process. This step of the process consisted on using both a DPSS CW laser and a mercury vapor lamp to adjust the positions of the optical elements in order to improve resolution and define the device's spectral range. At this point, a resolution of 3 nm was achieved with approximately the desired spectral range and a signal strength of $\sim 80\%$ of saturation at an integration time of 100 µs for the DPSS laser spectrum.

The final step in the production of the device is the calibration in terms of wavelength and intensity. The wavelength calibration resulted in a set of three parameters for a second-order polynomial to match the wavelength to the corresponding pixel on the detector. This model predicts the data with $R^2 = 0.99998$. From this calibration we obtain the spectral range of the prototype, $[950.5 - 1722.5]$nm, which can later be adjusted to better match the set requirement. The intensity calibration of the device was performed by dividing the acquired spectrum from a white light lamp by the theoretical model of a black body at $T = 2900$ K, which results in a calibration number for each pixel.

After the calibration of the device, we proceeded to analyze the results of acquiring different spectra. In terms of resolution, we were able to obtain a peak width of less than the required 3 nm, across the whole spectral range. We observed how the binning effect - having a discrete number of pixels on the detector - affect the resolution in some cases. We then used two different light sources - the mercury vapor lamp and a fluorescent lamp - to compare the developed prototype with a state of the art spectrometer. We conclude that both devices obtain similar spectra both in terms of wavelength calibration and intensity.

Finally, we verified all the mandatory requirements. Here, we leave for future work the design of a more compact version of the detector control PCB, the integration of an external trigger signal and the further development of a self-managed software library to control the device. Nevertheless, the developed spectrometer has already been successfully integrated in a fully operational d-scan product.

Chapter 6

Final Remarks

The d-scan technique by Sphere Ultrafast Photonics is an enabling technology for several areas of modern research and industry since it allows for the characterization and optimization of ultrashort laser pulses. The technique requires the use of somewhat expensive components such as a high precision translation stage and an InGaAs spectrometer. It also benefits from the implementation of a trigger signal to be used with low repetition rate lasers. The aim of this masters thesis was to develop custom versions of those devices, enabling the manufacturing of a low-cost d-scan product, and to implement the trigger feature using a custom designed PCB.

In Chapter 2 we introduce the relevant aspects to understanding the motivation of this thesis, going through the physics behind ultrashort pulses and introducing the concept of dispersion compensation with a d-scan product. In this chapter we also provide an analysis on the aspects required to develop a custom high precision translation stage such as the travel range, resolution and size. A similar analysis is performed on NIR InGaAs spectrometers, introducing concepts such as the spectral range and resolution. A market research is performed both on high resolution translation stages and on NIR spectrometers. This analysis, together with the needs of a d-scan product, provides a basis for the definition of the development requirements for such products.

Chapter 3 offers insight on the design process of custom PCBs which aim to implement a trigger signal on the d-scan products. The result of the process shows the successful implementation of the opto-isolation of the input trigger signal, the conversion of this signal from TTL to LVTTL and the implementation of a LED driver, in a compact and easy to integrate board. By extensively testing the device, we conclude that it fulfils all

the set requirements. Because of this, we were already successful in integrating these PCBs in several d-scan products thus enabling the trigger feature for the devices.

Chapter 4 details the development of a high precision translation stage. Requirements are set for the minimum travel range of the device (50 mm), the minimum step length (100 µm) and the direct integration of a glass wedge pair for the d-scan application, among others. The architecture of the device is defined according to these requirements by opting for a manual stage of sufficient travel range (65 mm) and screw lead (0.8 mm/rev) which will be coupled to a stepper motor. The chosen motor is capable of fulfilling the stepping resolution requirement by allowing for 200 steps/rev. We also decided that the control for the stage shall be provided by an Arduino Nano with an A4988 stepper motor controller. CNC parts were designed to fit all the components on a single assembly which supports mounting on a metric optical table and direct use with a glass wedge pair with angles of either 5° or 10°. A control PCB was also designed to provide a manual control knob for the stage and a *home* position calibration sensor. We developed a *C++* library featuring the sufficient methods to be used with the existing d-scan software. The translation stage was tested by performing both an interferometric measure and by performing d-scans of an ultrafast Ti:Sapph oscillator. We found that the stage was able to perform the interferometric measurements with an error of 7.46 %, on average, when considering the expected distance between maxima of the interference pattern. On the other hand, the data shows a 23.5 % standard deviation from the mean, when using the minimum step length of the stage. However, this instability is expected to be much lower for larger step lengths of the stage. This was later confirmed by the performed d-scans which provided an average 2 % RMS error and consistently retrieved a pulse width of around 8.58 fs and a pulse peak power of over 95 %. Finally, it is worth noting that the cost of this device was kept under the budget of 500 €. We can thus say that the development was successful and the device could be used with the d-scan technique, in the near future.

Chapter 5 shows the development process of a high resolution InGaAs spectrometer. The main requirements for the device were to have a spectral range in the NIR region of $[900 - 1700]$nm and a spectral resolution of 3 nm. To achieve this, *Matlab* ray tracing simulations were run to establish the geometry of the device. Custom mounts were designed to make the design as compact as possible. After developing a *C++* library to control the spectrometer, we assembled the prototype and began the tuning process. By using a DPSS CW laser and a Mercury vapor lamp as reference light sources, we reached the

required 3 nm resolution with a signal strength of ∼80 % of saturation at an integration time of 100 µs for the DPSS laser. We then performed a wavelength calibration of the device with a second-order polynomial model resulting in an R^2 of 0.99998. From this, we retrieved the spectral range of the device, $[950.5 - 1722.5]$nm, which is within the required specifications. An intensity calibration was also performed, using a white light lamp and the theoretical model of a black body at the temperature of the lamp, 2900 K. We then observed spectra from different light sources and concluded that the required 3 nm resolution was achieved across the whole spectral range. A comparison was made between the developed device and a state of the art InGaAs spectrometer showing that the spectra acquired by both devices agree, to a good extent, in terms of wavelength calibration and intensity. Note that, even though the two devices have a similar resolution, the developed spectrometer has a spectral range approximately 35 % larger than the one on the state of the art device. It is also important to mention that this device is extremely compact, having a size of 120 mm × 75 mm × 47 mm. Finally, the total cost of this device was kept under the budget of 3500 €.

Future work can be performed in further characterizing the mechanical robustness of the translation stage, resulting in a measure of its expected lifetime in travel distance, and on improving the compactness of the spectrometer by redesigning the control PCB for the InGaAs sensor.

Overall, I believe that this thesis achieved the proposed objectives. We were able to add the trigger feature to several d-scan devices, developed a translation stage which is compact, easy to integrate in a d-scan product and capable of performing well when used with the technique and demonstrated a very compact, high resolution, InGaAs spectrometer, that has since been integrated in a fully operational d-scan product.

Appendix A

Requirements Tables

A.1 Trigger PCB

A.1.1 Definition

#	Requirement	Description	Priority
1	Power Conversion	Implement a DC-DC converter capable of converting a 12 V or 15 V input to 5 V.	Mandatory
2	Trigger Input	Implement a TTL trigger signal input using a *Hirose U.FL* coaxial connector.	Mandatory
3	Timing delay	The PCB should introduce a maximum delay of 1 µs on the trigger signal.	Mandatory
4	Opto-isolation	Implement a circuit based on an opto-coupler to isolate the input trigger signal from the instruments under control.	Mandatory
5	Signal Conversion	Convert the TTL signal to Low-Voltage TTL (LVTTL).	Mandatory
6	LED Driver	Implement an LED driver for the intensity calibration of spectrometers in a d-scan product.	Mandatory
7	Size	Achieve dimensions of less than 50 mm × 60 mm × 6 mm for the component populated board.	Mandatory

#	Requirement	Description	Priority
8	Mounting Holes	Implement at least two M3 mounting holes for securing the PCB to the product	Mandatory
9	GPIO Pin Interface	Implement an interface with the GPIO pins on the instruments under control.	Desired

TABLE A.1: Technical requirements for the development of a trigger PCB.

A.1.2 Fulfilment

#	Requirement	Achieved
1	Power Conversion	Yes. Using external DC-DC converter.
2	Trigger Input	Yes.
3	Timing Delay	Yes. Tested for range [0.1Hz - 1MHz].
4	Opto-isolation	Yes.
5	Signal Conversion	Yes.
6	LED Driver	Yes.
7	Size	Yes.
8	Mounting Holes	Yes.
9	GPIO Pin Interface	Yes.

TABLE A.2: Fulfilment of the set requirements for the development of a trigger PCB.

A.2 High Precision Translation Stage

A.2.1 Definition

#	Requirement	Description	Priority
1	Resolution	Achieve a minimum step length of 100 µm.	Mandatory
2	Travel Range	Support a travel range of at least 50 mm.	Mandatory
3	Maximum Speed	Achieve a maximum stepping speed of 20 mm/s.	Mandatory
4	Size	Achieve a total footprint of less than 185.0 mm $\times$ 75.0 mm.	Mandatory
5	Communication Interface	Support communication with a computer through a *USB* connection and a *C++* library.	Mandatory
6	Optical Table Support	Support use with metric optical tables, at the glass wedge angles of 5° and 10°.	Mandatory
7	Glass Wedge Support	Integrate the mounting of the glass wedges directly on the stage base and moving platform.	Mandatory
8	Home Calibration	Support *home* position calibration.	Mandatory
9	Manual Control	Support the use of a knob as a manual control of the movement of the stage, when power is connected.	Mandatory
10	Price	Keep the total cost of the device, including the controller, under 500 €.	Desirable

TABLE A.3: Technical requirements for the development of a high precision translation stage.

A.2.2 Fulfilment

#	Requirement	Achieved	State of the Art
1	Resolution	Yes. $\sim$250 nm.	47 nm. Overdefined for this particular application.
2	Travel Range	Yes. 65 mm.	50 mm.
3	Maximum Speed	Acceptable for the application. Not quantified.	7 mm/s.
4	Size	Yes, within an acceptable margin. 186.3 mm $\times$ 74.4 mm.	172.9 mm $\times$ 65.0 mm.
5	Communication Interface	Yes. *USB*.	*RS-232 / USB.*
6	Optical Table Support	Yes. At 5 ^{o} and 10 ^{o} angles.	No direct support for mounting at a custom angle.
7	Glass Wedge Support	Yes. Direct integration.	Requires additional custom parts.
8	Home Calibration	Yes.	Yes.
9	Manual Control	Yes.	Yes.
10	Price	Yes. $<$500 €.	More than 3x as much.

TABLE A.4: Fulfilment of set requirements for the development of a high precision translation stage.

A.3 High Resolution InGaAs Spectrometer

A.3.1 Definition

#	Requirement	Description	Priority
1	Spectral Range	Support a wavelength range of $[900 - 1700]$ nm.	Mandatory
2	Resolution	Achieve a resolution of 3 nm.	Mandatory
3	Size	Achieve dimensions no more than 85.0 mm $\times$ 125.0 mm $\times$ 50.0 mm.	Mandatory
4	Optical Fiber Connector	Support SMA optical fiber input.	Mandatory
5	Cost	Keep the total cost of the device under a budget of 3500 €.	Mandatory
6	Software	Self managed library to interface with a *Windows* computer.	Desired
7	External Trigger	Support external TTL trigger.	Desired

TABLE A.5: Technical requirements for the development of an InGaAs spectrometer.

A.3.2 Fulfilment

#	Requirement	Achieved	State of the Art
1	Spectral Range	Yes. $[950.5 - 1722.5]$nm.	$\sim [900 - 1400]$nm.
2	Resolution	Yes. $\sim$3 nm.	$\sim$3 nm.
3	Size	Yes. 75.0 mm $\times$ 120.0 mm.	70.5 mm $\times$ 104.0 mm.
4	Optical Fiber Connector	Yes.	Yes.
5	Cost	Yes. $<$3500 €.	More than 2x as much.
6	Software	Yes. Can control device but not manage the USB connection.	Yes.
7	External Trigger	Not implemented.	Yes.

TABLE A.6: Fulfilment of the set requirements for the development of an InGaAs spectrometer.

Bibliography

[1] T. H. Maiman, "Stimulated optical radiation in ruby," *Nature*, 1960.

[2] O. Swenson and V. Marinov, "21 - laser processing of direct-write nano-sized materials," in *Advances in Laser Materials Processing*, ser. Woodhead Publishing Series in Welding and Other Joining Technologies, J. Lawrence, J. Pou, D. Low, and E. Toyserkani, Eds. Woodhead Publishing, 2010, pp. 671 – 694. [Online]. Available: http://www.sciencedirect.com/science/article/pii/B9781845694746500202

[3] C. TP, G. R, M. A, G. NT, de Souza RG, and B. SJ, "Advances in femtosecond laser technology," *Clinical Ophthalmology*, 2016.

[4] M. Miranda, T. Fordell, C. Arnold, A. L'Huillier, and H. Crespo, "Simultaneous compression and characterization of ultrashort laser pulses using chirped mirrors and glass wedges," *Opt. Express*, vol. 20, no. 1, pp. 688–697, Jan 2011. [Online]. Available: http://www.opticsexpress.org/abstract.cfm?URI=oe-20-1-688

[5] A. M. Weiner, *Ultrafast Optics*, G. Boreman, Ed. Wiley, 2009.

[6] E. Treacy, "Optical pulse compression with diffraction gratings," *IEEE Journal of Quantum Electronics*, vol. 5, pp. 454–458, Sep. 1969.

[7] D. Strickland and G. Mourou, "Compression of amplified chirped optical pulses," *Optics Communications*, vol. 56, no. 3, pp. 219 – 221, 1985. [Online]. Available: http://www.sciencedirect.com/science/article/pii/0030401885901208

[8] M. Rumpel, M. Moeller, C. Moormann, T. Graf, and M. A. Ahmed, "Broadband pulse compression gratings with measured 99.7% diffraction efficiency," *Opt. Lett.*, vol. 39, no. 2, pp. 323–326, Jan 2014. [Online]. Available: http://ol.osa.org/abstract.cfm?URI=ol-39-2-323

[9] R. Szipöcs, K. Ferencz, C. Spielmann, and F. Krausz, "Chirped multilayer coatings for broadband dispersion control in femtosecond lasers," *Opt. Lett.*, vol. 19, no. 3, pp. 201–203, Feb 1994. [Online]. Available: http://ol.osa.org/abstract.cfm?URI=ol-19-3-201

[10] Thorlabs, "Chirped mirrors," https://www.thorlabs.com/newgrouppage9.cfm?objectgroup_id=3746.

[11] S. Rausch, T. Binhammer, A. Harth, J. Kim, R. Ell, F. Kärtner, and U. Morgner, "Controlled waveforms on the single-cycle scale from a femtosecond oscillator," *Optics express*, vol. 16, pp. 9739–45, 07 2008.

[12] P. Dombi, V. S. Yakovlev, K. O'Keeffe, T. Fuji, M. Lezius, and G. Tempea, "Pulse compression with time-domain optimized chirped mirrors," *Opt. Express*, vol. 13, no. 26, pp. 10 888–10 894, Dec 2005. [Online]. Available: http://www.opticsexpress.org/abstract.cfm?URI=oe-13-26-10888

[13] A. Stingl, C. Spielmann, F. Krausz, and R. Szipöcs, "Generation of 11-fs pulses from a ti:sapphire laser without the use of prisms," *Opt. Lett.*, vol. 19, no. 3, pp. 204–206, Feb 1994. [Online]. Available: http://ol.osa.org/abstract.cfm?URI=ol-19-3-204

[14] Thorlabs, "Hene lasers: Red," https://www.thorlabs.com/newgrouppage9.cfm?objectgroup_id=1516.

[15] Newport, "Hene lasers," https://www.newport.com/c/hene-lasers.

[16] Coherent, "Mephisto lasers," https://www.coherent.com/lasers/main/mephisto-lasers.

[17] E. Huggins, "Teaching the uncertainty principle in introductory physics," http://ftp.aip.org/epaps/phys_teach/E-PHTEAH-45-010701/Teaching%20Uncertainty%20Principle.pdf.

[18] Thorlabs, "Ti:sapphire femtosecond laser (<8 fs)," https://www.thorlabs.com/newgrouppage9.cfm?objectgroup_id=3163.

[19] Coherent, "Ti sapphire laser," http://lasers.coherent.com/lasers/Ti-Sapphire-Laser.

[20] R. Weigand, M. Miranda, and H. Crespo, "Oscilador láser de titanio:zafiro de 2 ciclos ópticos," *Optica Pura y Aplicada*, vol. 46, pp. 105–110, 06 2013.

[21] J. K. LL.D., "Xl. a new relation between electricity and light: Dielectrified media birefringent," *The London, Edinburgh, and Dublin Philosophical Magazine and Journal of Science*, vol. 50, no. 332, pp. 337–348, 1875. [Online]. Available: https://doi.org/10.1080/14786447508641302

[22] A. Yefet, S.; Pe'er, "A review of cavity design for kerr lens mode-locked solid-state lasers," *Applied Sciences*, 2013.

[23] J.-C. M. Diels, J. J. Fontaine, I. C. McMichael, and F. Simoni, "Control and measurement of ultrashort pulse shapes (in amplitude and phase) with femtosecond accuracy," *Appl. Opt.*, vol. 24, no. 9, pp. 1270–1282, May 1985. [Online]. Available: http://ao.osa.org/abstract.cfm?URI=ao-24-9-1270

[24] D. Kane and R. Trebino, "Characterization of arbitrary femtosecond pulses using frequency-resolved optical gating," *Quantum Electronics, IEEE Journal of*, vol. 29, pp. 571 – 579, 03 1993.

[25] P. O'Shea, M. Kimmel, X. Gu, and R. Trebino, "Highly simplified device for ultrashort-pulse measurement," *Opt. Lett.*, vol. 26, no. 12, pp. 932–934, Jun 2001. [Online]. Available: http://ol.osa.org/abstract.cfm?URI=ol-26-12-932

[26] I. Amat-Roldán, I. G. Cormack, P. Loza-Alvarez, E. J. Gualda, and D. Artigas, "Ultrashort pulse characterisation with shg collinear-frog," *Opt. Express*, vol. 12, no. 6, pp. 1169–1178, Mar 2004. [Online]. Available: http://www.opticsexpress.org/abstract.cfm?URI=oe-12-6-1169

[27] G. Stibenz and G. Steinmeyer, "Interferometric frequency-resolved optical gating," *Opt. Express*, vol. 13, no. 7, pp. 2617–2626, Apr 2005. [Online]. Available: http://www.opticsexpress.org/abstract.cfm?URI=oe-13-7-2617

[28] C. Iaconis and I. A. Walmsley, "Spectral phase interferometry for direct electric-field reconstruction of ultrashort optical pulses," *Optics Letters 23*, 1998.

[29] D. R. Austin, T. Witting, and I. A. Walmsley, "Resolution of the relative phase ambiguity in spectral shearing interferometry of ultrashort pulses," *Opt. Lett.*, vol. 35, no. 12, pp. 1971–1973, Jun 2010. [Online]. Available: http://ol.osa.org/abstract.cfm?URI=ol-35-12-1971

[30] A. S. Wyatt, A. Grün, P. K. Bates, O. Chalus, J. Biegert, and I. A. Walmsley, "Accuracy measurements and improvement for complete characterization of optical pulses from nonlinear processes via multiple spectral-shearing interferometry," *Opt. Express*, vol. 19, no. 25, pp. 25 355–25 366, Dec 2011. [Online]. Available: http://www.opticsexpress.org/abstract.cfm?URI=oe-19-25-25355

[31] A. S. Wyatt, I. A. Walmsley, G. Stibenz, and G. Steinmeyer, "Sub-10 fs pulse characterization using spatially encoded arrangement for spectral phase interferometry for direct electric field reconstruction," *Opt. Lett.*, vol. 31, no. 12, pp. 1914–1916, Jun 2006. [Online]. Available: http://ol.osa.org/abstract.cfm?URI=ol-31-12-1914

[32] J. R. Birge, R. Ell, and F. X. Kärtner, "Two-dimensional spectral shearing interferometry for few-cycle pulse characterization," *Opt. Lett.*, vol. 31, no. 13, pp. 2063–2065, Jul 2006. [Online]. Available: http://ol.osa.org/abstract.cfm?URI=ol-31-13-2063

[33] V. V. Lozovoy, I. Pastirk, and M. Dantus, "Multiphoton intrapulse interference. iv. ultrashort laser pulse spectral phase characterization and compensation," *Opt. Lett.*, vol. 29, no. 7, pp. 775–777, Apr 2004. [Online]. Available: http://ol.osa.org/abstract.cfm?URI=ol-29-7-775

[34] P. A. Franken, A. E. Hill, C. W. Peters, and G. Weinreich, "Generation of optical harmonics," *Phys. Rev. Lett.*, vol. 7, pp. 118–119, Aug 1961. [Online]. Available: https://link.aps.org/doi/10.1103/PhysRevLett.7.118

[35] R. Crystals, "Ktp for shg (second harmonic generation)," http://raicol.com/ktp/ktp-for-shg.

[36] M. Miranda, C. L. Arnold, T. Fordell, F. Silva, B. Alonso, R. Weigand, A. L'Huillier, and H. Crespo, "Characterization of broadband few-cycle laser pulses with the d-scan technique," *Opt. Express*, vol. 20, no. 17, pp. 18 732–18 743, Aug 2012. [Online]. Available: http://www.opticsexpress.org/abstract.cfm?URI=oe-20-17-18732

[37] O. Rodenko, P. Tidemand-Lichtenberg, and C. Pedersen, "Low repetition rate 343 nm passively q-switched solid-state laser for time-resolved fluorescence spectroscopy," *Opt. Express*, vol. 26, no. 16, pp. 20 614–20 621, Aug 2018. [Online]. Available: http://www.opticsexpress.org/abstract.cfm?URI=oe-26-16-20614

[38] Z. R. Man Jiang, B. Lu, T. Guo, L. Wan, Y. Zhang, and J. Bai, "Low-repetition-rate high-energy passively q-switched nd:yag solid laser based on graphene saturable absorber operating at 1064nm," *Current Nanoscience*, 2012.

[39] S. Kühn, M. Dumergue, S. Kahaly, S. Mondal, M. Füle, T. Csizmadia, B. Farkas, B. Major, Z. Várallyay, E. Cormier, M. Kalashnikov, F. Calegari, M. Devetta, F. Frassetto, E. Månsson, L. Poletto, S. Stagira, C. Vozzi, M. Nisoli, P. Rudawski, S. Maclot, F. Campi, H. Wikmark, C. L. Arnold, C. M. Heyl, P. Johnsson, A. L'Huillier, R. Lopez-Martens, S. Haessler, M. Bocoum, F. Boehle, A. Vernier, G. Iaquaniello, E. Skantzakis, N. Papadakis, C. Kalpouzos, P. Tzallas, F. Lépine, D. Charalambidis, K. Varjú, K. Osvay, and G. Sansone, "The ELI-ALPS facility: the next generation of attosecond sources," *Journal of Physics B: Atomic, Molecular and Optical Physics*, vol. 50, no. 13, p. 132002, jun 2017. [Online]. Available: https://doi.org/10.1088%2F1361-6455%2Faa6ee8

[40] M. Miranda, P. Rudawski, C. Guo, F. Silva, C. Arnold, T. Binhammer, H. Crespo, and A. L'Huillier, "Ultrashort laser pulse characterization from dispersion scans: a comparison with spider," in *CLEO: 2013*, 01 2013, p. JTh2A.31.

[41] F. Silva, M. Miranda, B. Alonso, J. Rauschenberger, V. Pervak, and H. Crespo, "Simultaneous compression, characterization and phase stabilization of gw-level 1.4 cycle vis-nir femtosecond pulses using a single dispersion-scan setup," *Opt. Express*, vol. 22, no. 9, pp. 10 181–10 191, May 2014. [Online]. Available: http://www.opticsexpress.org/abstract.cfm?URI=oe-22-9-10181

[42] F. Böhle, M. Kretschmar, A. Jullien, M. Kovacs, M. Miranda, R. Romero, H. Crespo, U. Morgner, P. Simon, R. Lopez-Martens, and T. Nagy, "Compression of CEP-stable multi-mJ laser pulses down to 4 fs in long hollow fibers," *Laser Physics Letters*, vol. 11, no. 9, p. 095401, jun 2014. [Online]. Available: https://doi.org/10.1088%2F1612-2011%2F11%2F9%2F095401

[43] F. Calegari, G. Sansone, S. Stagira, C. Vozzi, and M. Nisoli, "Advances in attosecond science," *Journal of Physics B: Atomic, Molecular and Optical Physics*, vol. 49, no. 6, p. 062001, feb 2016. [Online]. Available: https://doi.org/10.1088%2F0953-4075%2F49%2F6%2F062001

[44] H. Marroux, A. Fidler, D. Neumark, and S. Leone, "Multidimensional spectroscopy with attosecond extreme ultraviolet and shaped near-infrared pulses," *Science Advances*, vol. 4, p. eaau3783, 09 2018.

[45] H. Timmers, Y. Kobayashi, K. F. Chang, M. Reduzzi, D. M. Neumark, and S. R. Leone, "Generating high-contrast, near single-cycle waveforms with third-order dispersion compensation," *Opt. Lett.*, vol. 42, no. 4, pp. 811–814, Feb 2017. [Online]. Available: http://ol.osa.org/abstract.cfm?URI=ol-42-4-811

[46] D. Guenot, D. Gustas, A. Vernier, B. Beaurepaire, F. Böhle, M. Bocoum, M. Lozano, A. Jullien, R. Lopez-Martens, A. Lifschitz, and J. Faure, "Relativistic electron beams driven by khz single-cycle light pulses," *Nature Photonics*, 03 2017.

[47] C. Maibohm, F. Silva, E. Figueiras, P. T. Guerreiro, M. Brito, R. Romero, H. Crespo, and J. B. Nieder, "Syncrgb-flim: synchronous fluorescence imaging of red, green and blue dyes enabled by ultra-broadband few-cycle laser excitation and fluorescence lifetime detection," *Biomed. Opt. Express*, vol. 10, no. 4, pp. 1891–1904, Apr 2019. [Online]. Available: http://www.osapublishing.org/boe/abstract.cfm?URI=boe-10-4-1891

[48] F. Silva, B. Alonso, W. Holgado, R. Romero, J. S. Román, E. C. Jarque, H. Koop, V. Pervak, H. Crespo, and I. nigo J. Sola, "Strategies for achieving intense single-cycle pulses with in-line post-compression setups," *Opt. Lett.*, vol. 43, no. 2, pp. 337–340, Jan 2018. [Online]. Available: http://ol.osa.org/abstract.cfm?URI=ol-43-2-337

[49] BWTEK, "Spectral resolution," http://bwtek.com/spectrometer-part-5-spectral-resolution/.

[50] OceanOptics, "How does my choice of spectrometer slit size affect optical resolution?" https://oceanoptics.com/faq/choice-slit-size-affect-resolution/.

[51] J.-C. Diels and W. Rudolph, *Ultrashort Laser Pulse Phenomena*, A. Press, Ed. Academic Press, 1996.

[52] Hamamatsu, "S1337-1010br," https://www.hamamatsu.com/eu/en/product/type/S1337-1010BR/index.html.

[53] ——, "G11620-512da," https://www.hamamatsu.com/eu/en/product/type/G11620-512DA/index.html.

[54] Hirose, "U.fl series coaxial connectors," https://www.hirose.com/product/series/U.FL.

[55] C. N. Danson, C. Haefner, J. Bromage, T. Butcher, J.-C. F. Chanteloup, E. A. Chowdhury, A. Galvanauskas, L. A. Gizzi, J. Hein, D. I. Hillier, and et al., "Petawatt and exawatt class lasers worldwide," *High Power Laser Science and Engineering*, vol. 7, p. e54, 2019.

[56] L. Lavenu, M. Natile, F. Guichard, X. Délen, M. Hanna, Y. Zaouter, and P. Georges, "High-power two-cycle ultrafast source based on hybrid nonlinear compression," *Opt. Express*, vol. 27, no. 3, pp. 1958–1967, Feb 2019. [Online]. Available: http://www.opticsexpress.org/abstract.cfm?URI=oe-27-3-1958

[57] SparkFun, "Sparkfun electronics eagle rules," https://www.sparkfun.com/tutorial/Eagle-DFM/EagleRules.pdf.

[58] Pololu, "A4988 stepper motor driver carrier," https://www.pololu.com/product/1182.

[59] McMaster-Carr, "Set screw precision flexible shaft coupling," https://www.mcmaster.com/9861t525.

[60] Arduino, "Arduino nano," https://store.arduino.cc/arduino-nano.

[61] Honeywell, "Linear hall-effect sensor ics: Ss490 series," https://sensing.honeywell.com/honeywell-sensing-sensors-linear-hall-effect-ics-ss490-series-datasheet-005843-2-en.pdf.

[62] J. Rodrigues, "Mechatronics platforms for micron-level positioning and sensing: applications to femtosecond laser diagnostics and laser marking," 2018, final Report as part of the PEEC program in FCUP.

[63] caiuspetronius, "Optometrika," https://github.com/caiuspetronius/Optometrika.

[64] EdmundOptics, "Short wave uv quartz pencil lamp," https://www.edmundoptics.com/p/short-wave-uv-quartz-pencil-lamp/4640/.